Received: 12 November 2019 | Revised: 13 December 2019 | Accepted: 6 January 2020

DOI: 10.1002/pld3.200

ORIGINAL RESEARCH

Chlamydomonas reinhardtii as a plant model system to study mitochondrial complex I dysfunction

Nitya Subrahmanian[1,2] | **Andrew David Castonguay**[1,3] | **Thea Aspelund Fatnes**[1] | **Patrice Paul Hamel**[1,4]

[1]Department of Molecular Genetics, The Ohio State University, Columbus, OH, USA

[2]Plant Cellular and Molecular Biology Graduate Program, The Ohio State University, Columbus, OH, USA

[3]Molecular Genetics Graduate Program, The Ohio State University, Columbus, OH, USA

[4]Department of Biological Chemistry and Pharmacology, The Ohio State University, Columbus, OH, USA

Correspondence
Patrice Paul Hamel, Department of Molecular Genetics, Department of Biological Chemistry and Pharmacology, The Ohio State University, Room 582 Aronoff Laboratory, 318 W. 12th Avenue, Columbus, OH 43210, USA.
Email: hamel.16@osu.edu

Present address
Thea Aspelund Fatnes, Fürst Medical Laboratory, Oslo, Norway

Funding information
United Mitochondrial Disease Foundation

Abstract

Mitochondrial complex I, a proton-pumping NADH: ubiquinone oxidoreductase, is required for oxidative phosphorylation. However, the contribution of several human mutations to complex I deficiency is poorly understood. The unicellular alga *Chlamydomonas reinhardtii* was utilized to study complex I as, unlike in mammals, mutants with complete loss of the holoenzyme are viable. From a forward genetic screen for complex I-deficient insertional mutants, six mutants exhibiting complex I deficiency with assembly defects were isolated. *Chlamydomonas* mutants isolated from our screens, lacking the subunits NDUFV2 and NDUFB10, were used to reconstruct and analyze the effect of two human mutations in these subunit-encoding genes. The K209R substitution in NDUFV2, reported in Parkinson's disease patients, did not significantly affect the enzyme activity or assembly. The C107S substitution in the NDUFB10 subunit, reported in a case of fatal infantile cardiomyopathy, is part of a conserved C-$(X)_{11}$-C motif. The cysteine substitutions, at either one or both positions, still allowed low levels of holoenzyme formation, indicating that this motif is crucial for complex I function but not strictly essential for assembly. We show that the algal mutants provide a simple and useful platform to delineate the consequences of patient mutations on complex I function.

KEYWORDS

Chlamydomonas reinhardtii, complex I, insertional and site-directed mutagenesis, mitochondrial biogenesis, mitochondrial diseases

1 | INTRODUCTION

Mitochondrial oxidative phosphorylation (OXPHOS) involves four major membrane-bound complexes (I, II, III, and IV) mediating electron transfer from the substrates, NADH or succinate, to the terminal electron acceptor O_2 (Green & Tzagoloff, 1966). In concert with their oxidoreductase activities, complexes I, III, and IV also translocate protons across the mitochondrial inner membrane, thereby establishing the proton gradient necessary for complex V (F_1F_0 ATP synthase) to generate ATP on the matrix side (Mitchell, 1961).

With over 40 nucleus- and mitochondria-encoded subunits, mitochondrial complex I is a type-I NADH dehydrogenase (Kerscher,

Dröse, Zickermann, & Brandt, 2008) and the largest respiratory complex in the mitochondrial inner membrane (Hirst, 2013). Among the ~40 subunits common to all eukaryotic complexes I (Cardol, 2011), only 14 orthologs make up the bacterial enzyme and are therefore considered to be the "core" subunits as they constitute the minimal requirement for enzymatic activity (Berrisford, Baradaran, & Sazanov, 2016). This highly conserved core is composed of seven catalytic subunits often encoded by the nuclear genome, binding the prosthetic groups (one FMN and eight iron-sulfur (Fe-S) clusters) required for oxidation of NADH, plus seven hydrophobic subunits (ND subunits) generally encoded in the mitochondrial genomes of eukaryotes (Remacle, Barbieri, Cardol, & Hamel, 2008). The roles of the 24 non-core subunits conserved in all eukaryotic lineages, also referred to as "accessory subunits," are largely unknown. It is proposed that they have supportive roles in stabilizing the complex and/or regulating its activity (Kmita & Zickermann, 2013; Stroud et al., 2016).

Complex I biogenesis in eukaryotes is a complicated process dependent upon the coordinated expression of the nuclear and mitochondrial genomes (Guerrero-Castillo et al., 2017). This process has attracted considerable attention as ~37% of OXPHOS disorders are characterized by isolated or combined complex I deficiency (Ghezzi & Zeviani, 2018; Rodenburg, 2016). Since the first report of human complex I deficiency by Morgan-Hughes *et al*. in 1979, pathogenic mutations have been discovered in 20 (out of 37) nuclear-encoded subunits and all seven mitochondrially encoded subunits of complex I (Fiedorczuk & Sazanov, 2018; Friederich et al., 2017; Koopman et al., 2016; Rodenburg, 2016). These mutations have been associated with a variety of clinical symptoms including hypertrophic cardiomyopathy, Leigh syndrome, and additional neurodegenerative disorders (Koopman et al., 2016; Pagniez-Mammeri et al., 2012; Sharma, Lu, & Bai, 2009). At the cellular level, patient-derived fibroblasts display a diverse range of phenotypes including decreased complex I activity and assembly, increased reactive oxygen species production, mitochondrial membrane depolarization, defective ATP production, and altered mitochondrial morphology (Distelmaier et al., 2009; Giachin, Bouverot, Acajjaoui, Pantalone, & Soler-Lopez, 2016).

Although our knowledge of complex I deficiency is broadening, the molecular mechanisms underlying the clinical symptoms remain poorly understood. There is no clear correlation between the clinical presentation and the corresponding molecular defects (Distelmaier et al., 2009). For instance, different mutations in the same gene may present with alternate clinical phenotypes. In addition, there is variability in the complex I deficiency observed at the tissue and organ levels for the same patient (Giachin et al., 2016; Shoubridge, 2001). As the heterogeneity of the biochemical and clinical phenotypes adds additional layers of complexity, demonstrating the pathogenicity of a molecular lesion in humans has become a real challenge. Therefore, some mutations have been assigned a "provisional" status because their contribution to the disease phenotype remains uncertain (Mitchell, Elson, Howell, Taylor, & Turnbull, 2006).

Due to the above-mentioned difficulties associated with studying complex I disorders, non-human experimental model systems have been used to dissect the molecular bases of mitochondrial complex I assembly. While bacterial systems have been previously used for reconstructing human pathogenic mutations, they lack the subunit complexity of their eukaryotic counterpart (Vinothkumar, Zhu, & Hirst, 2014). Similarly, the single-celled eukaryote *Saccharomyces cerevisiae* is an unsuitable experimental system because it lacks mitochondrial complex I (Lasserre et al., 2015). Previously, the obligate aerobic yeasts *Yarrowia lipolytica* and *Neurospora crassa* have been successfully utilized to mimic disease-associated mutations in genes encoding structural subunits and an assembly factor (Ahlers, Garofano, Kerscher, & Brandt, 2000; Duarte, Schulte, Ushakova, & Videira, 2005; Kerscher, Grgic, Garofano, & Brandt, 2004; Maclean, Kimonis, & Balk, 2018).

The unicellular photosynthetic alga *Chlamydomonas reinhardtii* (to be referred to as *Chlamydomonas*) has emerged as an alternative simple model system for studying mitochondrial complex I (Barbieri et al., 2011; Remacle et al., 2008; Salinas, Larosa, Cardol, Marechal-Drouard, & Remacle, 2014). Firstly, the composition of complex I in *Chlamydomonas* is similar to its human counterpart (Cardol et al., 2004, 2008; Remacle, Hamel, Larosa, Subrahmanian, & Cardol, 2012). Secondly, the nuclear and mitochondrial genomes encoding complex I subunits are amenable to manipulation (Barbieri et al., 2011; Remacle, Cardol, Coosemans, Gaisne, & Bonnefoy, 2006). Thirdly, unlike mammalian organisms, complete loss of complex I is still viable due to the capacity of this alga to photosynthesize (Cardol et al., 2003; Massoz et al., 2015).

In addition, alternative enzymes in the *Chlamydomonas* electron transport chain (ETC) can partially bypass the lack of complex I (Lecler, Vigeolas, Emonds-Alt, Cardol, & Remacle, 2012), thereby allowing respiratory growth due to which complex I mutants display a characteristic slow-growth-in-the-dark (SID) phenotype. In a previous study by our group, a forward genetic screen conducted based on the SID phenotype led to the isolation of seven nuclear mutants, *amc1* to *amc7* (for *a*ssembly of *m*itochondrial *c*omplex I) defining six distinct loci required for complex I function (Barbieri et al., 2011). In this study, we report the description of *amc8* to *amc13* which were also uncovered via insertional mutagenesis. Among these mutants, the *amc5* and *amc9* mutations were mapped to nuclear genes encoding the complex I subunits NUOB10 (NDUFB10 in human) and NUO5 (NDUFV2 in human), respectively (Barbieri et al., 2011 and this study), proving the efficacy of our screen. We have utilized *Chlamydomonas* complex I mutants *amc5* (*nuob10/ndufb10-null*) and *amc9* (*nuo5/ndufv2-null*) as a platform for determining the pathogenicity of human mutations in the genes encoding NDUFB10 and NDUFV2, respectively. The human mutations were reconstructed in *Chlamydomonas*, and their effect on complex I activity and assembly were assessed.

2 | MATERIALS AND METHODS

2.1 | Strains and culture conditions

Chlamydomonas strains were grown in Tris-acetate-phosphate (TAP), with Hutner's trace elements, 20 mM Tris base and 17 mM acetic acid,

or TAP supplemented with arginine (1.9 mM) (TARG), TARG supplemented with 25 μg/ml hygromycin B (TARG + HyB), or 25 μg/ml paromomycin (TARG + Pm) liquid or solid medium at 25°C in continuous light at 50 μmol m^{-2} s^{-1} (Harris, 1989). In accordance with our laboratory conditions, we define high light conditions as 50 μmol m^{-2} s^{-1} and low light conditions correspond to 0.5 μmol m^{-2} s^{-1}. Solid medium contains 1.5% (w/v) select agar (Invitrogen, 30391049). The background strains used to generate transformants were $3A^+$ (*mt*$^+$; *arg7-8*) [CC-5589] and $4C^-$ (*mt*$^-$; *arg7-8*) [CC-5590] (Dr. Rochaix, University of Geneva). The strains 141 (*arg9-2*; *mt*$^+$), CC-124 (*mt*$^-$), CC-125 (*mt*$^+$), or 1′ (*mt*$^+$) [a *137C* derivative, provided by Dr. Claire Remacle, University of Liège, Belgium] were used in crosses and/or as experimental controls. Strains *amc5* (87D3) [CC-5591], *dum11* [CC-4098], and *dum18* were used in this study (Barbieri et al., 2011; Remacle, Duby, Cardol, & Matagne, 2001a). Insertional mutagenesis and phenotypic screening of complex I mutants are detailed in Method S1. Genetic analyses are described in Method S2. Ten-fold dilution series and growth curve analyses were conducted as described in Method S3.

Saccharomyces cerevisiae strain CW04 (*MATα ade2-1 his3-11,15 leu2-3,11 trp1-1 ura3-1*; Banroques, Delahodde, & Jacq, 1986) was utilized for plasmid construction via gap repair (Method S5) and grown at 28°C in synthetic dextrose medium containing all amino acids (SD + AA) prior to plasmid construction. Colonies carrying the recombinant plasmids were selected in synthetic dextrose medium lacking only uracil (*SD*-ura) (Dujardin, Pajot, Groudinsky, & Slonimski, 1980). Chemo-competent *Escherichia coli* DH5α strains were used for molecular cloning. *E. coli* was grown at 37°C in Luria-Bertani (LB) broth and agar (Silhavy, Berman, & Enquist, 1984).

2.2 | TAIL-PCR and PCR-based screening of indexed cosmid library

Nucleic acid extraction, diagnostic PCRs, and real-time quantitative PCRs were conducted as in Method S4.

TAIL-PCR (thermal asymmetric inter-laced PCR) was conducted to identify the sequence flanking the iHyg3 cassette (encoding the *APHVII* gene conferring hygromycin B resistance) in the *amc9* mutant as in Liu, Mitsukawa, Oosumi, and Whittier (1995) using the partially degenerate primer AD1 (Dent, Haglund, Chin, Kobayashi, & Niyogi, 2005; Liu et al., 1995; Table S1). The following iHyg3-specific primers, APH7R3, APH7R4, and APH7R5 (Table S1), were used for the primary, secondary, and tertiary TAIL-PCRs, respectively. Similar reactions were conducted using wild-type genomic DNA and purified iHyg3 cassette to identify non-specific amplification of DNA.

Cosmids containing *NUO5* and *NUOB10* genomic DNA were identified by PCR (Purton & Rochaix, 1994). The *NUO5*-containing cosmid (referred to as 9A2) was identified using the primer pairs NUO5 E2L/NUO5 E3R (Table S1). The *NUOB10*-containing cosmid (referred to as cosmid 7D10) was identified using the primer pairs NUOB10E1L/NUOB10E4R (Table S1). The borders of *Chlamydomonas* genomic DNA inserted into these cosmids were sequenced to confirm the presence of genomic region including the gene of interest.

2.3 | Biolistic transformation

The list of plasmids and recipient strains used for biolistic transformation is provided in Method S5 and Tables S2, S3, and S4. The recipient strains *amc9 (41D9) (mt*$^-$; *nuo5::APHVII*; *arg7-8)* [CC-5601] or *amc5 (87D3) (mt*$^+$; *nuob10::APHVIII*; *arg7-8)* [CC-5591] were subjected to biolistic transformation using a homemade particle delivery device. The recipient strain was grown in liquid TARG medium for 2–3 days until it reached the exponential phase (3–6 × 10^6 cells/ml). The cells were plated on respective selective medium at 10^8 cells/plate. For each bombardment, DNA was coated on sterile 0.6–0.9 μm tungsten particles (Strem Chemicals, # 93–7437) by using 2 μg of transforming DNA, 16.7 mM spermidine, and 1 M $CaCl_2$. The bombardment was conducted at a helium pressure of 1.725 MPa and vacuum of ~92 kPa. The plate was positioned 10.5 cm away from the particle-containing nozzle. The bombarded plates were first incubated at 0.5 μmol m^{-2} s^{-1} light overnight for recovery and then transferred to continuous light (50 μmol m^{-2} s^{-1}). Transformants containing cosmids with the *ARG7* marker (9A2 for *amc9* and 7D10 for *amc5*) were selected based on arginine prototrophy. Transformants containing the mutant genes were selected based on their respective antibiotic resistance (Table S4) and were subsequently screened for the presence of the transgene by diagnostic PCR. The site-directed mutations in each selected transformant were confirmed by sequencing.

2.4 | Complex I activity measurements

Mitochondrial enzymatic activity measurements were conducted as described previously in Cardol, Matagne, and Remacle (2002), Remacle, Baurain, Cardol, and Matagne (2001b), Remacle, Gloire, Cardol, and Matagne (2004), with slight modifications. Cells grown for 2–3 days on solid medium were harvested and resuspended in MOPS-KOH extraction buffer (10 mM MOPS-KOH pH 7.4, 0.5 M mannitol, 100 mg/ml BSA, 0.5 mM PMSF). Cells were lysed by sonication using a Branson Sonifier 150 (1/8 inch probe tip), at 12 W output for 2 × 30 s. Following lysis, the extract was centrifuged at 480 *g* for 10 min, followed by 3,000 *g* for 5 min. The supernatant was centrifuged at 27,000 *g* for 20 min, and the resulting pellet was the crude membrane extract. Complex I activity was determined as the rate of NADH oxidation, which was measured spectrophotometrically at 340 nm. The substrates used were 100 μM NADH (Amresco, 0384-1G) and 100 μM duroquinone (Aldrich, D22320-4). Specific activity was calculated using the molar extinction coefficient for NADH at ε_{340nm} = 6.22 mM^{-1} cm^{-1} in the absence and presence of 45 μM rotenone (MP Biomedicals, 150154), a complex I-specific inhibitor. Complex II + III and complex IV activity assays are described in Method S6.

2.5 | Blue-native PAGE (BN-PAGE) and in-gel activity assays

Partially purified membranes were extracted as described above for activity measurement. Complexes were separated

by BN-PAGE using 4%–12% (w/v) acrylamide gradient gels (Schägger & von Jagow, 1991). Membranes were partially solubilized as follows. Membrane proteins (500 µg) were pelleted at 18,000 *g* for 20 min at 4°C. The membranes were resuspended in 180 µl of 2% (w/v) sodium *n*-dodecyl-β-D maltoside (DDM; Bioworld, 40430017-3) and solubilized by incubating in DDM in wet ice for 1 hr, followed by addition of 20 µl of 10% (w/v) sodium taurodeoxycholate hydrate (TDC; Sigma, T-0875). Both DDM and TDC were dissolved in ACA buffer (750 mM aminocaproic acid, 0.5 mM EDTA, 50 mM Bis-Tris, pH 7). Partially solubilized membrane proteins (200 µg) were loaded per lane. *In-gel* NADH dehydrogenase (complex I) activity was visualized as purple bands after incubating the gels in 100 mM MOPS-KOH buffer, pH 8, containing 1 mg/ml *p*-nitro blue tetrazolium chloride (NBT; GoldBio, NBT2.5) and 0.2 mM NADH. Following *in-gel* complex I staining, *in-gel* ATPase (complex V) activity was detected by incubating the gels overnight in the dark, in 50 mM HEPES-KOH pH 8 buffer containing 30 mM $CaCl_2$ and 8.2 mM ATP (Fisher Bioreagents, BP413-25), until a white precipitate was visible. This precipitate revealed the ATPase activity of complex V. Coomassie staining was conducted for loading control. Immunoblotting methods are detailed in Method S7.

3 | RESULTS

3.1 | Isolation of novel complex I mutants via forward genetics

To uncover additional *AMC* loci, insertional mutagenesis was conducted using the 4C$^-$ wild-type strain (*mt*$^-$; *arg7-8*) as the recipient and the iHyg3 cassette, encoding the *APHVII* gene that confers hygromycin B resistance (HyB^R), as transforming DNA. The resulting transformants were screened by replica plating for the SID phenotype, a characteristic phenotype of complex I deficiency in *Chlamydomonas* (Remacle, Baurain, et al., 2001b). Among 4,200 insertional mutants, six *amc* mutants (*amc8* to *amc13*) displaying a SID phenotype (Figure 1a) and deficient in rotenone-sensitive NADH: duroquinone oxidoreductase activity (Figure 1b), were isolated. While the *amc8*, *amc9*, and *amc11* strains had severely decreased complex I activity, the *amc10*, *amc12*, and *amc13* exhibited partial complex I deficiency. To test whether the mutation in the *amc* strains yielded defects in other respiratory enzymes, we measured complex II + III and IV activities (Figure 1c). Apart from *amc12*, all the *amc* mutants exhibited elevated complex II + III activity, a common feature previously observed in several *Chlamydomonas* complex I mutants (Barbieri et al., 2011; Cardol et al., 2002; Remacle, Baurain, et al., 2001b). None of the *amc* mutants, except *amc12*, displayed a defect in complex IV activity (Figure 1d). We concluded that all *amc* mutants, with the exception of *amc12*, displayed isolated complex I deficiency. The *amc12* mutant was pleiotropic with defects in complexes I, II + III, and IV.

3.2 | The complex I mutants display defects in complex I assembly

To assess the level of complex I assembly in the newly isolated *amc* mutants, protein complexes from crude membrane extracts were separated via BN-PAGE (blue-native polyacrylamide gel electrophoresis). Mature complex I (~950 kDa) and partially assembled subcomplexes were visualized by *in-gel* staining that reveals NADH dehydrogenase activity as a purple band (Figure 2a). Note that complex I mutants with an assembled soluble arm are capable of *in-gel* NADH oxidation, even if the ubiquinone reductase activity is impaired. Based on the *in-gel* activity, we categorized the *amc* strains into four groups: (a) no active complex I in the *amc9* mutant, (b) accumulation of a subcomplex displaying NADH dehydrogenase activity in the *amc11* strain, (c) decreased levels of active complex in *amc8 and amc12*, and (d) wild-type levels of *in-gel* NADH dehydrogenase activity in *amc10* and *amc13* strains. BN-PAGE immunoblotting analysis (Figures 2b and S1) showed that no assembled complex I was detected in *amc9*, whereas fully assembled complexes accumulating to a lesser degree than wild-type were observed for *amc8*, *amc10*, *amc12*, and *amc13*. The highly labile subcomplex observed in *amc11* is indicative of a defect in assembling the distal membrane arm of complex I (Barbieri et al., 2011; Cardol et al., 2008).

It has been previously observed that some complex I mutants accumulate reduced levels of complex I subunits as a result of impaired holoenzyme assembly (Barbieri et al., 2011; Saada et al., 2008). Hence, the steady-state accumulation of a subset of complex I subunits was examined by SDS-PAGE immunoblotting analysis (Figure 2c). Three subunits from the soluble arm of complex I, 49 kDa (NUO7), 51 kDa (NUO6), and TYKY (NUO8) (Barbieri et al., 2011; Cardol, 2011), were chosen for analysis based on the availability of antibodies. Only *amc8*, *amc11*, and *amc12* accumulated reduced levels of 49 kDa, 51 kDa, and TYKY subunits, whereas *amc10* and *amc13* accumulated these subunits to wild-type levels. The *amc9* mutant displayed decreased levels of the 51 kDa subunit.

3.3 | The *amc9*, *amc11*, and *amc12* mutations are linked to the insertional marker

Although the complex I mutants were generated by insertional mutagenesis, previous genetic analyses of *amc* mutants showed that the insertional cassette is not always linked to complex I deficiency (Barbieri et al., 2011). The unlinked mutations could be due to the insertion of extracellular genomic DNA uptaken during electroporation (Zhang et al., 2014), insertion of cleaved and non-functional pieces of the cassette, or insertion of the random herring sperm DNA used as part of the electroporation protocol (Shimogawara, Fujiwara, Grossman, & Usuda, 1998). Hence, genetic analyses were conducted to determine the nature of the *amc* mutations. Analysis of the heterozygous diploid progeny (*amc*/+) showed the diploids were restored for growth in the dark, indicating that all *amc* mutations were recessive for the complex

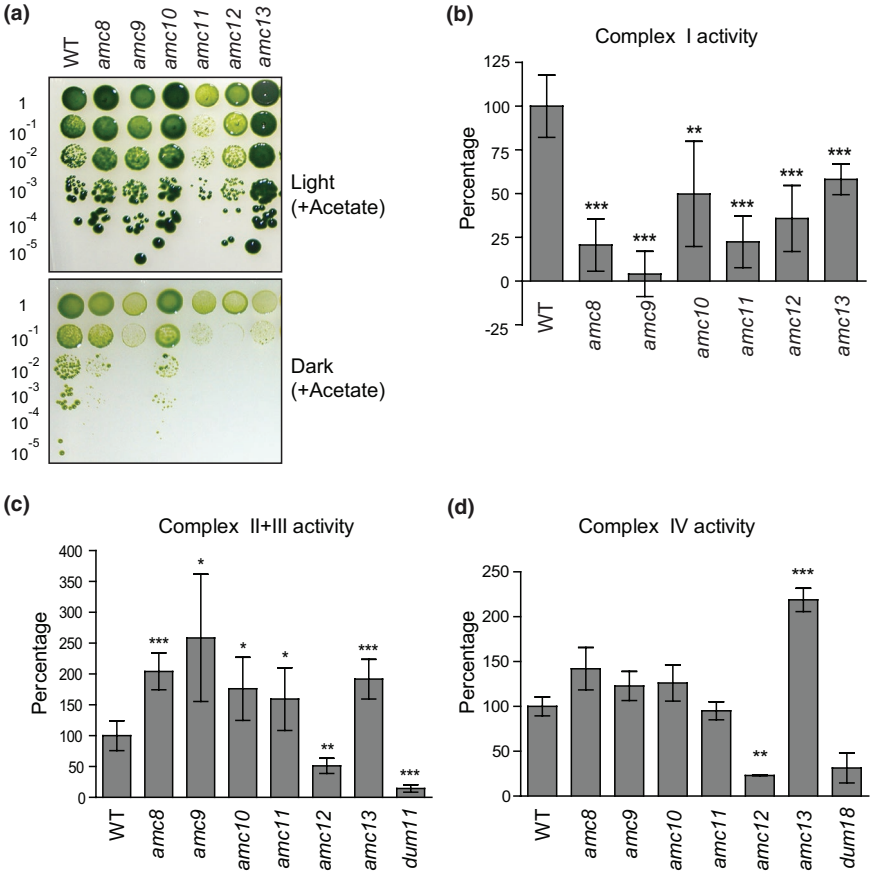

FIGURE 1 The *amc8* to *amc13* mutants exhibit complex I deficiency. (a) The growth phenotype of the wild-type (WT, 4C⁻) and *amc8* to *amc13* mutants was analyzed by 10-fold dilution series. The dilutions were plated on medium containing acetate as a carbon source and incubated in continuous light or in the dark for 20 days. In (b), (c), and (d), the enzymatic activities were conducted on crude membrane extracts and are displayed as percentage of the activity mean of WT, with the error bars indicating percentage of standard deviation of the mean. WT strain used for comparison is 4C⁻ for the *amc* strains and CC-124 for *dum11* and *dum18*. Statistical significance was determined by two-tailed unequal variances *t* test. * indicates $p < .05$, ** indicates $p < .01$, and *** indicates $p < .001$. (b) Complex I (rotenone-sensitive NADH: duroquinone oxidoreductase) activity was determined from six independent biological replicates. The average complex I activity of WT was 46.6 ± 8.3 nmol NADH oxidized. min^{-1} mg^{-1} protein. (c) Complex II + III (succinate: cytochrome *c* oxidoreductase) activity was assessed from six independent biological replicates (except *amc8* for which five biological replicates were used). The WT displayed an activity of 18.1 ± 4.3 nmol of cytochrome *c* reduced. min^{-1} mg^{-1} protein. A mutant displaying complex III deficiency (*dum11*) was used as a control. (d) Complex IV activity (cytochrome *c* oxidase) was determined from three independent biological replicates. The WT displayed an activity of 269.6 ± 28.6 nmol of cytochrome *c* oxidized. min^{-1} mg^{-1} protein. A mutant displaying complex IV deficiency (*dum18*) was used as a control. In all the figures, the original mutant strains were used except for *amc10 (12C)* and *amc13 (16)* (in a, c, and d), which are derivatives of the original *amc10* and *amc13* mutants

I-deficient phenotype (Figure S2). Meiotic progeny of *amc* × wild-type crosses were tested to determine whether the *amc* mutations were monogenic and the insertional cassette co-segregated with the complex I-deficient phenotype (Table 1). The analyses indicated that the complex I deficiency in the *amc8*, *amc9*, *amc10*, *amc11*, and *amc13* strains exhibited monogenic inheritance (Table 1). In addition, all the HyB^R meiotic progeny, derived from genetic crosses of wild-type, with *amc9*, *amc11*, or *amc12*, displayed a SID phenotype, indicating that the complex I deficiency in these mutants is tightly linked to the insertional cassette. On the other hand, for *amc8*, *amc10*, *and amc13*, only a fraction of the HyB^R recombinant meiotic progeny displayed the SID phenotype, indicating that the *AMC* locus responsible for the complex I-deficient phenotype was segregating away from the antibiotic resistance insertional cassette. Tetrad analysis also confirmed that the complex I deficiency was not linked to the insertional cassette in the *amc10* and *amc13* mutants. We conclude that the recessive complex I deficiency in the *amc* mutants was linked to the insertional cassette only for *amc9*, *amc11*, and *amc12*. In this study, we show further characterization of the *amc9* mutant.

3.4 | The *amc9* mutation maps to the *NUO5* gene encoding the 24 kDa subunit of complex I

In the case of *amc9*, analyses of seven tetrads and 50 HyB^R recombinant meiotic progeny obtained from bulk germination of meiotic zygotes showed that the antibiotic resistance always segregated with

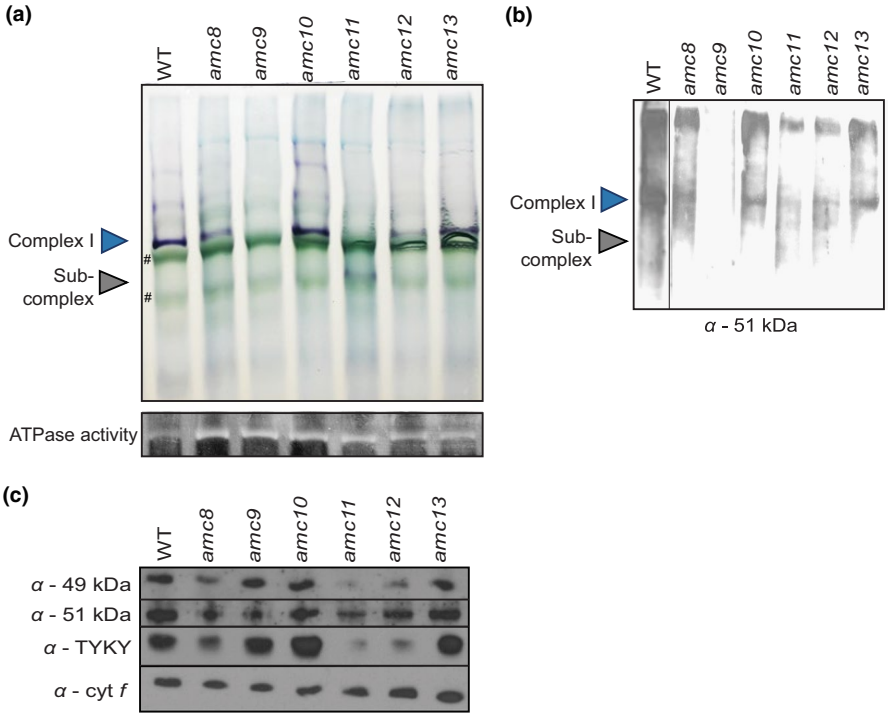

FIGURE 2 The *amc* mutants display a complex I assembly defect. (a and b) BN-PAGE (blue-native polyacrylamide gel electrophoresis) was conducted on 200 μg of partially purified membrane fraction. (a, *Top panel) In-gel* complex I activity was detected by NBT staining. The purple bands indicate *in-gel* staining of NADH dehydrogenase activity in mature (950 kDa) and partially assembled subcomplexes of complex I. In some cases, multiple purple bands larger than 950 kDa are detected, which could be due to partially solubilized membranes or might correspond to complex I in association with other complexes (Cardol et al., 2008). The symbol (#) indicates the photosynthetic complexes present in the crude membrane extract, migrating at sizes similar to that of the complex I holoenzyme and the subcomplex. They are marked only in two lanes for ease of reference. (a, *Bottom panel) In-gel* ATPase staining to detect complex V was conducted to verify quality of crude membrane preparation and loading. The reduced ATPase staining in WT compared to the *amc* mutants was not systematically observed. (b) Immunoblotting was conducted, using α-51 kDa antibody, on complexes separated by BN-PAGE to detect the assembled soluble arm of complex I. This image is a composite of two gels run on the same day as indicated with a black vertical line: with the WT lane from one gel and the lanes corresponding to the *amc* mutants from another. (c) SDS-PAGE immunoblotting was conducted on 10 μg of partially purified membranes using polyclonal antibodies to detect soluble arm complex I subunits: α-49 kDa, α-51 kDa, α-TYKY. α-cyt *f* was used to confirm equal loading. In (a) and (b), WT is the 4C$^-$ strain and the *amc8* to *amc13* strains are the original mutants except the *amc10 (12C)* strain, which is a meiotic progeny derived from the original *amc10* strain

the SID phenotype (Figure S3). The tight linkage between the insertional marker and the SID phenotype in the *amc9* mutant suggests that the disruption of a gene controlling complex I, by the insertional cassette, could be responsible for the complex I deficiency. To identify the disrupted gene in the *amc9* mutant, we sought to recover the genomic sequence flanking the insertional cassette via TAIL-PCR (Liu et al., 1995). The full-length insertional cassette was mapped to exon 2 of the *NUO5* gene, which encodes the 24 kDa subunit (NUO5) of the soluble arm of complex I (Figure S4A,B) (Subrahmanian, Remacle, & Hamel, 2016). Real-time RT-qPCR (Figure S4C) showed that the *amc9* mutant lacked the full-length *NUO5* transcript. These results confirmed the insertion of a full-sized iHyg3 cassette into exon 2 of the *NUO5* gene in the *amc9* mutant.

To test whether the insertional mutation in the *NUO5* gene is responsible for the complex I defect, we transformed the *amc9* mutant with a cosmid containing the wild-type copy of *NUO5* (referred to as [*amc9*; *NUO5*]) and assessed the recovery of complex I function. The *NUO5* transcript levels were restored upon complementation with the wild-type *NUO5* gene (Figure S4C). Rescue of the growth phenotype in the [*amc9*; *NUO5*] strain was measured by assessing growth on solid medium and in liquid culture (Figures 3a,b and S4E). The generation time in the dark for wild-type and *amc9* was 17.5 hr and 52 hr, respectively, whereas the [*amc9*; *NUO5*] strain displayed a wild-type level of growth in the dark as evidenced by a generation time of 16.8 hr (Figure 3b). Further biochemical analyses of [*amc9*; *NUO5*] revealed wild-type levels of NADH: duroquinone oxidoreductase activity (Figure 3d), complex I subunits abundance (Figure S4D), and complex I assembly (Figure 3e,f). From these results, we conclude that the *AMC9* locus corresponds to the *NUO5* gene encoding the 24 kDa complex I subunit (referred to as NUO5 in *Chlamydomonas* and NDUFV2 in humans [Pagniez-Mammeri et al., 2012, Subrahmanian et al., 2016]).

3.5 | The NDUFV2 K209R variant does not affect complex I activity or assembly in *Chlamydomonas*

NDUFV2/NUO5 is the 24 kDa soluble subunit localized to the matrix arm of the holoenzyme (Figure 3c) and is one of the core

TABLE 1 Phenotypic and genetic analysis of the *amc* mutants

Strain	CI activity (%)	Fully assembled complex	Subcomplex	Genetic analysis	Recombinant meiotic progeny		Linkage to cassette	Monogenic
					Total	SID		
WT	100	++++	–	—	—	—	—	—
amc8	21	++	–	Bulk	230	50	No	Yes
amc9	4	–	–	Bulk, Tetrad	50	50	Yes	Yes
amc10	50	+++	–	Bulk, Tetrad	100	48	No	Yes
amc11	22	–	++	Bulk	100	100	Yes	Yes
amc12	36	++	–	Bulk	85	85	Yes	N.D.
amc13	58	+++	–	Bulk, Tetrad	112	51	No	Yes

Note: Complex I-specific activity for the *amc* mutants was determined by measuring rotenone-sensitive NADH: duroquinone oxidoreductase activity and is represented as percentage of WT activity (WT, $4C^{-}$ at 46.6 ± 8.3 nmol NADH oxidized. min^{-1} mg^{-1} protein, set to 100%). The detection of fully assembled complex and the subcomplex was determined from BN-PAGE (blue-native polyacrylamide gel electrophoresis) *in-gel* activity and immunoblotting. ++++, +++, ++, +, – indicate relative levels of detected complex. To test whether the *amc* mutations are monogenic, genetic analysis of the meiotic progeny of *amc* x wild-type crosses was performed by analyzing the 2:2 segregation of complex I phenotype in tetrads. In cases where tetrad analysis was not successful, bulk germination of zygotes was conducted and the resulting meiotic progeny were scored for complex I-deficient phenotype. In the case of *amc9*, *amc10*, and *amc13*, each of the tetrads that were tested showed a 2:2 segregation of the SID (slow growth in the dark) and wild-type heterotrophic growth phenotype, confirming monogenic inheritance of the complex I-deficient trait (Figure S3). In the case of the *amc12* mutant, the monogenic inheritance of the SID phenotype could not be determined (N.D.) via tetrad analysis due to poor germination of the zygotes.

subunits harboring a 2Fe-2S (N1a) cluster which is coordinated by four cysteines (Figure S5; Birrell, Morina, Bridges, Friedrich, & Hirst, 2013). As a highly conserved protein, human NDUFV2 displays 51% identity with the *Chlamydomonas* NUO5 ortholog (Figure S5) and is a known marker for complex I disorders (Pagniez-Mammeri et al., 2012). While the association of complex I deficiency with Parkinson's disease (PD) is a well-established phenomenon, the exact molecular mechanisms defining how specific complex I-related mutations cause pathogenesis have remained unclear (Giachin et al., 2016). One particular lysine-to-arginine (K209R) variant in NDUFV2 was detected in one out of 33 familial probands and one out of 238 sporadic PD cases (Nishioka et al., 2010). However, complex I enzymatic activity was not assessed in these patients to determine whether this mutation causes a complex I deficiency that may contribute to the development of PD.

In some cases, it has been shown that lysine-to-arginine substitutions may affect protein folding, and in others, it has been proposed that lysine-to-arginine substitutions increase stability through putative salt bridges and hydrogen bond formations (Sokalingam, Raghunathan, Soundrarajan, & Lee, 2012). To investigate the biochemical effect of the NDUFV2-K209R variant on complex I activity and assembly, the corresponding mutation was reconstructed in the gene encoding the *Chlamydomonas* NUO5 ortholog and the variant was expressed in the *nuo5-null* mutant strain *amc9*. This lysine residue is well-conserved in eukaryotic species and occurs at position 230 of *Chlamydomonas* NUO5 (yellow highlight, Figure S5). The sequence encoding either the wild-type or the K230R subunit was introduced into a construct containing the *NUO5* genomic DNA, fused to a sequence encoding a C-terminal FLAG-tag, under the control of the *NUO5* native promoter. Transformants were generated in the *amc9* strain via biolistics, and those accumulating the FLAG-tagged NUO5 protein were selected for further analyses (Figure S6).

The potential impact of the lysine-to-arginine substitution on growth was assessed (Figure 4a). As observed previously, the *amc9* mutant strain exhibited a SID phenotype whereas complementation with the wild-type *NUO5* gene or recombinant *NUO5* gene with a C-terminal FLAG-tag restored growth in the dark to wild-type levels. Interestingly, transformants expressing the K230R NUO5-FLAG variant also exhibited wild-type growth in the dark, indicating that this substitution in NUO5 does not affect respiratory growth (Figure 4a). Accordingly, NADH: duroquinone oxidoreductase activity was also restored by the K230R NUO5 variant (Figure 4b). To test the level of complex I assembly in the NUO5 lysine-to-arginine variant, complexes were separated by BN-PAGE and subjected to *in-gel* activity assays and immunoblotting (Figure 4c). The NUO5 subunit is part of the matrix arm responsible for NADH dehydrogenase activity. As a result, no mature complex I or subcomplexes were detected by *in-gel* activity or immunoblotting in the *amc9* mutant. Complementation with the wild-type *NUO5-FLAG* gene restored complex I assembly. In addition, immunoblotting with the α-51 kDa or α-FLAG antibodies showed that the NUO5-FLAG K230R variant was successfully incorporated into the holoenzyme. This was in agreement with detection of fully assembled complex I via *in-gel* activity assay showing that the NADH dehydrogenase activity of the soluble arm was restored. From these results, we conclude that the K230R substitution in NUO5, a candidate mutation for PD, does not affect complex I activity or assembly in *Chlamydomonas*.

3.6 | The *AMC5* locus corresponds to the NUOB10-encoding gene

NUOB10/NDUFB10/PDSW is an accessory subunit that is localized to the distal end of the membrane arm, although NUOB10 is hydrophilic

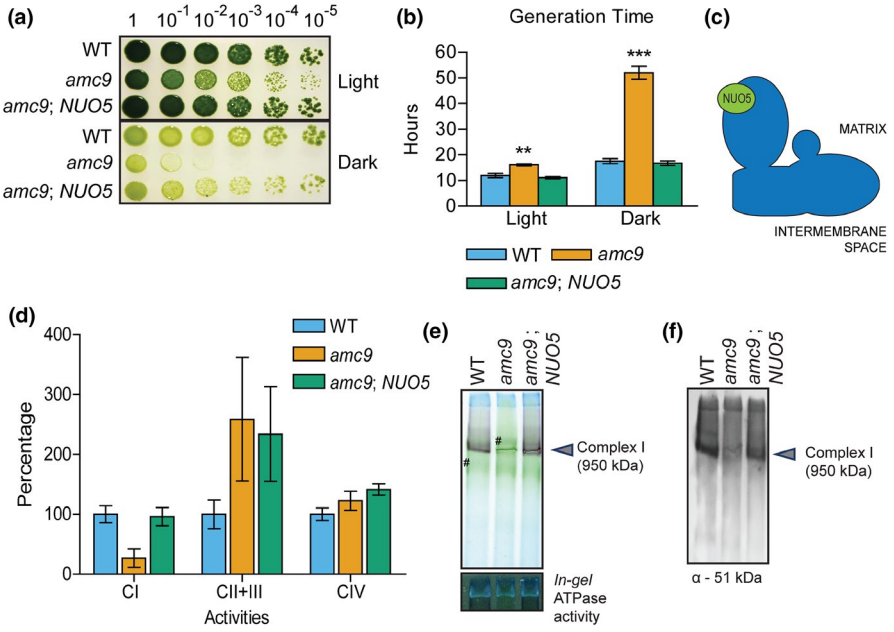

FIGURE 3 The *amc9* mutant, complemented by the *NUO5* gene, is restored for complex I activity and assembly. (a) Restoration of the growth phenotype in [*amc9*; *NUO5*] was tested by 10-fold dilution series plated on acetate-containing medium and incubated in the light for seven days and in the dark for 16 days. (b) The average generation time for each strain calculated from growth curves in Figure S4E is indicated here. The error bars represent standard deviation of the mean. Statistically significant difference with respect to the WT was determined by two-tailed unequal variances *t* test. ** indicates $p < .01$, and *** indicates $p < .001$. (c) The approximate location of the NUO5 subunit in the matrix arm of complex I is indicated in a diagrammatic representation. (d) Complex I (CI), complex II + III (CII + III), and complex IV (CIV) activities were determined on partially purified membranes. The activities are represented as percentage of WT calculated from an average, with the error bars indicating standard deviation of the mean. The averages for CI, CII + III, and CIV activities were determined from three, six, and three biological replicates, respectively. For the reference strain, WT (4C$^-$), average CI activity was 76.4 ± 19.9 nmol NADH oxidized. min^{-1} mg^{-1} protein, average CII + III activity was 18.1 ± 4.3 nmol cytochrome *c* reduced. min^{-1} mg^{-1} protein, and average CIV activity was 269.6 ± 28.6 nmol cytochrome *c* oxidized min^{-1} mg^{-1} protein. The *amc9* mutant displays a significant reduction in complex I activity with respect to WT, as determined by two-tailed unequal variances *t* test with a *p* value = .03. The [*amc9*; *NUO5*] strain is rescued for complex I activity. While there is no significant difference between activities measured for the WT and [*amc9*; *NUO5*] strains, there is a significant difference between *amc9* and [*amc9*; *NUO5*] with a $p = .019$. (e) BN-PAGE (blue-native polyacrylamide gel electrophoresis) was conducted on 200 μg of partially purified membrane fraction. *In-gel* complex I activity was detected by NBT staining. The symbol (#) indicates the chlorophyll-containing complexes present in the crude membrane extract. *In-gel* ATPase activity was detected with $CaCl_2$/ATP staining. (f) BN-PAGE followed by immunoblotting was conducted on 200 μg of partially purified membrane fraction using polyclonal antibody to detect the 51 kDa subunit of the soluble arm of complex I

and does not contain any predicted transmembrane helices (Hirst, Carroll, Fearnley, Shannon, & Walker, 2003) (Figures 5e and S7). It is predicted to face the intermembrane space (IMS) and presumably associated with the membrane through interactions with neighboring membrane subunits (Zhu et al., 2015a). The *Chlamydomonas* NUOB10 displays 13.5% identity with the human ortholog NDUFB10.

The *amc5* mutant harbors the insertional cassette in intron 3 of the *NUOB10* gene (Barbieri et al., 2011) accompanied by a deletion of the *NUOB10* genomic sequence downstream of the insertion site (Figure S8A,B). The *amc5* mutant displayed decreased rotenone-sensitive NADH: duroquinone oxidoreductase activity (Figure 5a) and exhibited the characteristic *sid* phenotype of complex I-deficient mutants in both liquid and solid medium (Figures 5b and S8D,E) with an average generation time of 69 hr in the dark, compared to 27 hr for the wild-type strain. Real-time RT-qPCR confirmed the loss of the wild-type *NUOB10* mRNA in the *amc5* mutant (Figure S8C). The *amc5* mutant displayed an accumulation of a subcomplex, migrating at a size similar to the ~700 kDa subcomplex previously observed in *Chlamydomonas* mitochondrial mutants defective for the distal membrane arm assembly of complex I (Cardol et al., 2008; Remacle et al., 2008; Figure 5c,d).

To test whether the mutation in *NUOB10* is indeed responsible for the complex I defect, the *amc5* mutant was transformed with a cosmid containing the *NUOB10* gene (Figures 5 and S8). Molecular analyses of the [*amc5*; *NUOB10*] transformant revealed the presence of the wild-type *NUOB10* gene and restoration of relative *NUOB10* transcript levels. The [*amc5*; *NUOB10*] strain also exhibited restoration of growth in the dark, complex I activity, and assembly. From these results, we conclude that the *AMC5* locus corresponds to the *NUOB10* gene and the NUOB10 subunit is necessary for complex I membrane arm assembly.

3.7 | The NUOB10 C-$(X)_{11}$-C motif is important for complex I activity and assembly

To date, only one patient has been reported with mutations in *NDUFB10*. The patient, born to non-symptomatic parents, exhibited

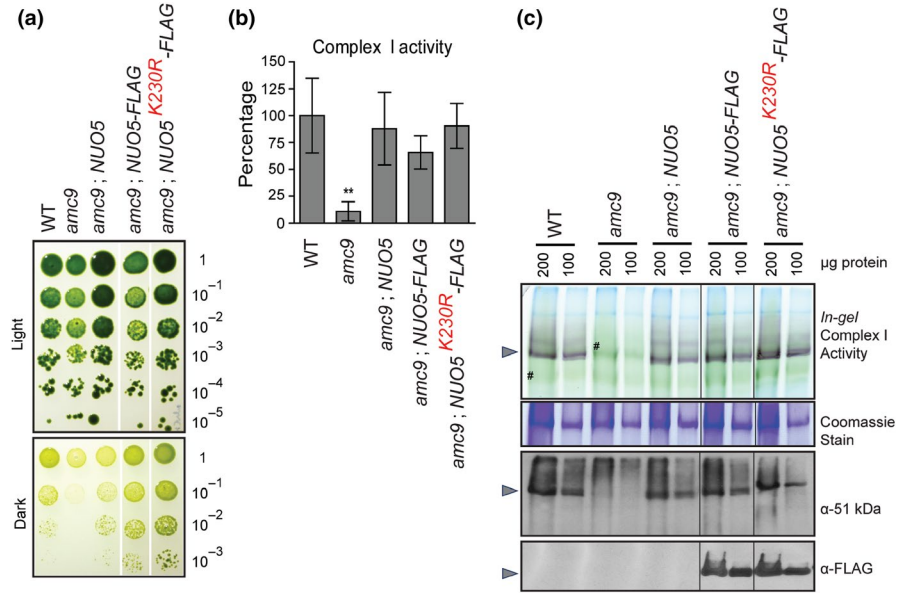

FIGURE 4 The lysine-to-arginine substitution in NUO5 does not affect complex I activity and assembly. (a) The growth phenotype of the WT and the *amc9* transformants was analyzed by 10-fold dilution series plated on acetate-containing medium and incubated in the light or in the dark for 14 days. White vertical lines indicate strains tested on the same plate and assembled together for this figure. (b) Complex I activity was determined with partially purified membranes from four biological replicates and represented as a percentage of WT average with the error bars indicating standard deviation of the mean. For WT (4C$^-$), average complex I activity was 71 ± 24.7 nmol NADH oxidized. min^{-1} mg^{-1} protein. The *amc9* mutant displayed a significant reduction in complex I activity with respect to WT, as determined by two-tailed unequal variances *t* test with a *p* value = 0.005. The [*amc9*; *NUO5-FLAG*] and the [*amc9*; *NUO5*^{K230R}*-FLAG*] transformants were restored for complex I activity. (c) BN-PAGE (blue-native polyacrylamide gel electrophoresis) was conducted on 200 µg and 100 µg of partially purified membrane fraction. *In-gel* complex I activity was detected by NBT staining. The gray arrowheads indicate fully assembled holoenzyme. The green bands (indicated with the symbol #) correlate to the co-purified photosynthetic complexes in the membrane fractions. Coomassie staining following BN-PAGE was used to test for equal loading. Protein(s) migrating at a size unrelated to complex I is shown here for this purpose. BN-PAGE followed by immunoblotting was conducted using a polyclonal antibody to detect the 51 kDa subunit of the soluble arm of complex I and a monoclonal α-FLAG antibody to detect NUO5-FLAG. Black vertical thin lines indicate lanes assembled together from the same gel/blot. The NUO5^{K230R}-FLAG is incorporated into the fully assembled complex I and allows wild-type levels of NADH dehydrogenase activity as detected by *in-gel* complex I activity assay

fetal cardiomyopathy and fatal infantile lactic acidosis, and died at 27 hr after birth (Friederich et al., 2017). Exome sequencing identified compound heterozygous sequence variation in the *NDUFB10* gene: (a) a paternally inherited nonsense mutation resulting in a premature stop codon, and (b) a maternally inherited missense mutation resulting in a cysteine-to-serine (C107S) substitution. This cysteine is part of a highly conserved C-(X)$_{11}$-C motif (yellow highlight, Figure S7), whose function in complex I activity and assembly has not been elucidated.

To understand the effect of the C107S substitution in NDUFB10 on complex I holoenzyme, we sought to reconstruct the corresponding mutation in the *Chlamydomonas nuob10*-null *amc5* mutant. The C107 residue in human NDUFB10 corresponds to the first cysteine of the C-(X)$_{11}$-C motif, at position 79 in the *Chlamydomonas* NUOB10 ortholog. To further gain insight into the role of the C-(X)$_{11}$-C motif in complex I activity, a cysteine-to-serine substitution at the second cysteine of the motif (C91S) and the double substitution (C79S-C91S) were also tested. For this purpose, the *NUOB10* genomic sequence (corresponding to wild-type, C79S, C91S, C79S-C91S variants) was fused to a sequence encoding a C-terminal FLAG-tag and expressed under the control of its native promoter. The *NUOB10* constructs were introduced into the *amc5/nuob10*-null mutant strain by biolistics. Transformants carrying the transgene were identified and chosen for further analyses (Figure S9A). To test the accumulation of NUOB10-FLAG in the transformants, immunoblotting was conducted. The NUOB10-FLAG variants were detected at the expected size of ~17 kDa with the α-FLAG antibody (Figure S9B).

The effect of the NUOB10 cysteine substitutions on respiratory growth was tested (Figure 6a). While the *amc5* recipient strain displayed a SID phenotype, transformants expressing the wild-type *NUOB10-FLAG* had restored growth in the dark similar to those with the *NUOB10*-containing cosmid. On the other hand, the single and double cysteine-to-serine variants displayed only partial restoration of growth in the dark. These observations indicate that while expression of the *NUOB10* variants can partially compensate for loss of NUOB10, manipulation of the C-(X)$_{11}$-C motif restricts respiratory growth.

To test the importance of the C-(X)$_{11}$-C motif for complex I activity and assembly, rotenone-sensitive NADH: duroquinone oxidoreductase activity and BN-PAGE *in-gel* activity were assessed (Figure 6b,c). The *amc5* strain transformed with wild-type *NUOB10-FLAG* showed rescue of complex I activity to ~65% of wild-type levels (Figure 6b). Although

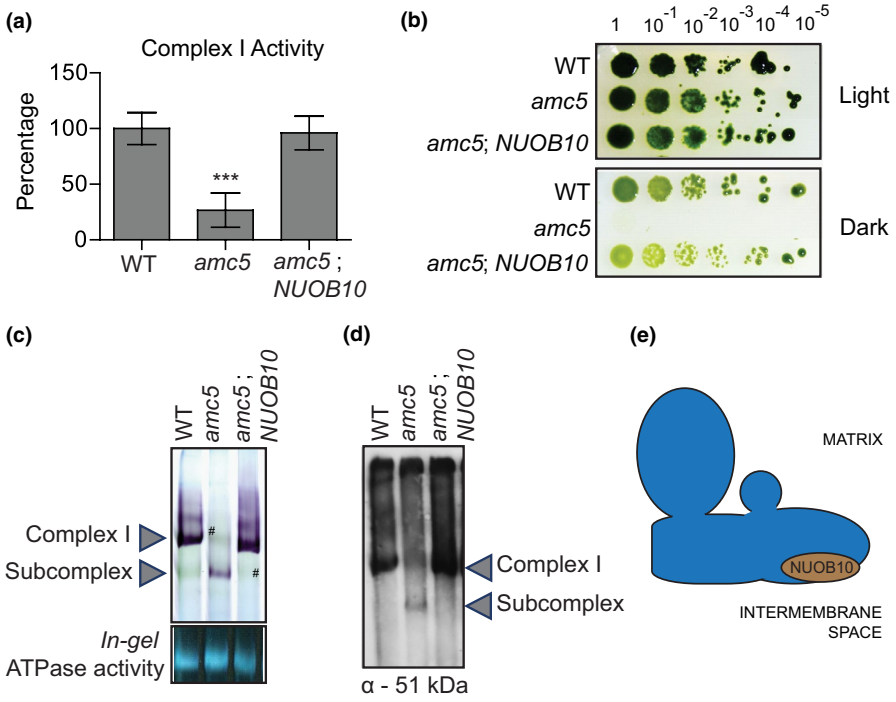

FIGURE 5 The *amc5* mutant phenotypes are rescued by the *NUOB10* gene. The *amc5* strain was transformed with a *NUOB10*-containing cosmid by biolistics. The phenotypic rescue of one representative transformant [*amc5*; *NUOB10*] is shown here. The WT and *amc5* strains shown here are $3A^{+}$ and *amc5 (87D3)*, respectively. (a) Complex I (rotenone-sensitive NADH: duroquinone oxidoreductase) activity was determined with partially purified membranes. The activities are represented as a percentage of the average of three biological replicates with the error bars indicating percentage of standard deviation of the mean. The average complex I activity of WT is 54.0 ± 7.7 nmol NADH oxidized. min^{-1} mg^{-1} protein. The activities for the WT and *amc5* strains are significantly different according to the two-tailed unequal variances *t* test with a $p = .000116$. The *amc5* and [*amc5*; *NUOB10*] strain have significantly different activities with a $p = .000199$. (b) Restoration of the growth phenotype in [*amc5*; *NUOB10*] was tested by 10-fold dilution series plated on acetate-containing medium and incubated in the light for seven days and in the dark for 16 days. (c and d) BN-PAGE was conducted on 200 μg of partially purified membranes. (c) *In-gel* complex I activity was detected by NBT staining, and *in-gel* ATPase activity was detected with $CaCl_2$/ ATP staining. Crude membrane extracts, also containing the photosynthetic membranes, were used for this analysis. The symbol (#) indicates examples of photosynthetic complexes migrating closely with complex I and subcomplex that can be clearly observed in their absence. (d) Immunoblotting was conducted using a polyclonal antibody to detect the 51 kDa subunit of complex I. (e) A diagrammatic representation of the L-shaped mitochondrial complex I, with the approximate location of the NUOB10/NDUFB10 subunit in the distal membrane arm facing the IMS (Zhu et al., 2015b)

the restoration of complex I activity for the [*amc5*; *NUOB10-FLAG*] transformant was not as high as with the [*amc5*; *NUOB10*] control strain, BN-PAGE *in-gel* activity and immunoblotting revealed wild-type levels of mature complex I at ~950 kDa, showing that the C-terminal FLAG-tag does not significantly impair complex I assembly (Figure 6c). On the other hand, the cysteine-to-serine single and double substitutions in NUOB10 yielded severe complex I deficiency, indicating that the C-$(X)_{11}$-C motif is crucial for complex I activity (Figure 6b). Interestingly, the accumulation of the 700 kDa subcomplex due to the loss of NUOB10 in the *amc5* mutant was attenuated in the presence of the NUOB10 variants (Figure 6c). Mature complex I (~950 kDa), absent in the *amc5* mutant, was detected in the single and double cysteine-to-serine variants via *in-gel* activity and immunoblotting with α-51 kDa. Immunoblotting with α-FLAG (detecting NUOB10) further revealed that the NUOB10 variants were incorporated into the mature complex. The restoration of complex I assembly, in spite of the cysteine-to-serine substitutions, could account for the slight improvement in the complex I activity levels of the cysteine-to-serine variants (~16% of wild-type) compared to the *amc5* mutant (~8% of wild-type) and partial rescue of the respiratory growth phenotype (Figure 6a,b). However, the NUOB10 variants failed to accumulate wild-type levels of mature complex I, as evidenced by immunoblotting (Figure 6b). The level of complex I assembly is similar for the single or double mutant variants, an indication that mutation of either or both cysteines of the C-$(X)_{11}$-C motif elicits the same impact on complex I activity and assembly. Additionally, the three distinct NUOB10-FLAG cysteine-to-serine variants accumulated to only 50% of wild-type (Figure S9B), indicating that the cysteines may also be required for the stability of NUOB10. From these observations, we concluded that the cysteines within the highly conserved C-$(X)_{11}$-C motif of NUOB10 play an important role in complex I assembly and activity.

4 | DISCUSSION

Mitochondrial complex I, the first and largest enzyme of the mitochondrial ETC, is a proton-pumping NADH: ubiquinone

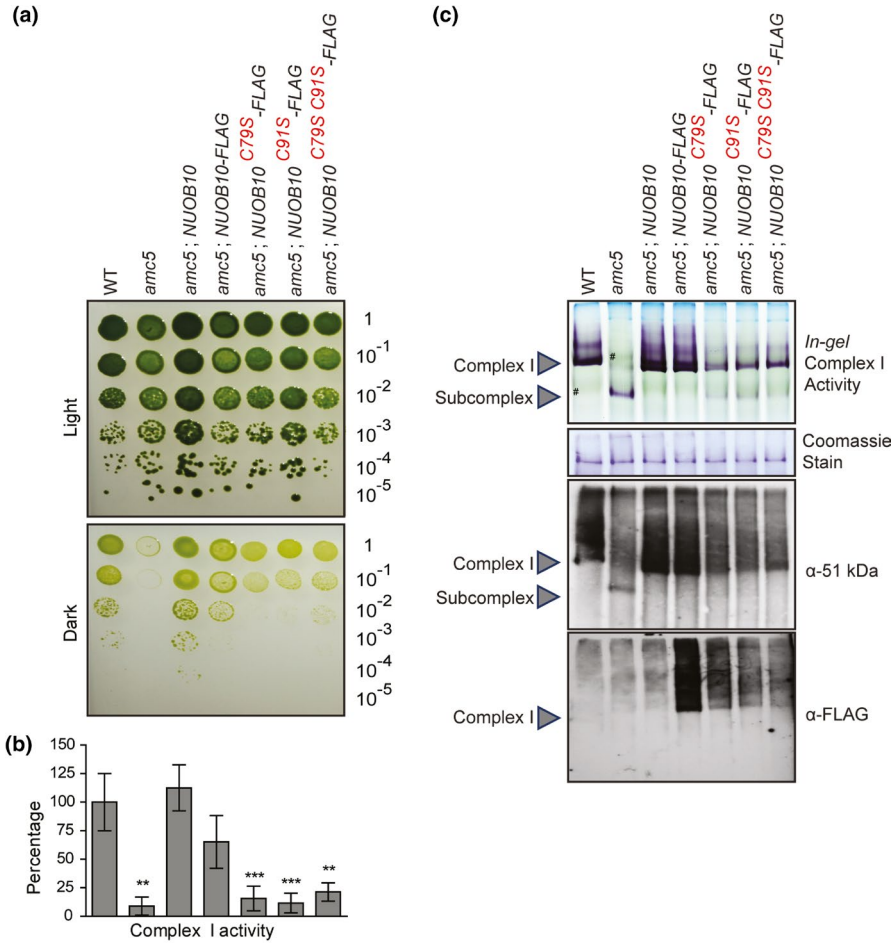

FIGURE 6 The cysteine-to-serine substitutions in NUOB10 decrease complex I activity and assembly. The *amc5* mutant was transformed with four constructs containing the *NUOB10* genomic DNA: (i) wild-type *NUOB10* sequence (*NUOB10* or *NUOB10-FLAG*), and mutant *NUOB10* sequences encoding the variants with (ii) the C79S substitution (*NUOB10*^{C79S}*-FLAG*), (iii) the C91S substitution (*NUOB10*^{C91S}*-FLAG*), or (iv) the C79S and C91S double substitutions (*NUOB10*^{C79SC91S}*-FLAG*). The wild-type (WT, 3A^{+}), *amc5* mutant, and [*amc5*; *NUOB10*] strains were used as controls. (a) The growth phenotype of the wild-type and *amc5* transformants was analyzed by 10-fold dilution series. The dilutions were plated on medium containing acetate as a carbon source and incubated in the light or in the dark for 14 days. (b) Complex I activities, conducted with partially purified membranes, are represented as percentage of WT calculated from the average of five biological replicates with the error bars indicating standard deviation of the mean. For WT, average complex I activity was 48.3 ± 12.1 nmol NADH oxidized. min^{-1} mg^{-1} protein. The *amc5* transformants producing the C79S, C91S, and C79SC91S variants display significantly reduced complex I activities compared to WT as determined by two-tailed unequal variances *t* test. ** indicates $p < .01$, and *** indicates $p < .001$. The graph is aligned to match with the labels in (a). (c) BN-PAGE was conducted on 200 µg of partially purified membrane proteins. *In-gel* complex I activity was detected by NBT staining. The symbol (#) indicates the photosynthetic complexes present in the crude membrane extract. Although present in all the lanes, they are marked only in two lanes for ease of reference. Coomassie staining serves as loading control, and protein(s) migrating at a size different from complex I is shown here. Immunoblotting was conducted using a polyclonal antibody to detect the 51 kDa subunit of the soluble arm of complex I and a monoclonal α-FLAG antibody to detect the NUOB10-FLAG

oxidoreductase (Remacle et al., 2012). In an effort to isolate novel mutants for unraveling complex I biogenesis, a forward genetic approach in *Chlamydomonas reinhardtii* was undertaken. In the first part of this study, we described the isolation of six complex I mutants *amc8* to *amc13*, in addition to the previously characterized *amc1* to *amc7* (Barbieri et al., 2011). We showed that, except for *amc12*, the *amc* mutants displayed isolated complex I deficiency (Figure 1) with various levels of assembly defects of the mutants (Table 1; Figure 2). The *amc9* mutation resulted in no detectable complex, whereas the *amc11* mutation caused the accumulation of a subcomplex—both indicative of the assembly process being prematurely aborted. On the other hand, *amc8*, *amc10*, *amc12*, and *amc13* mutants were capable of assembling a mature holoenzyme.

So far, the forward genetic screen conducted by our group has resulted in the isolation of 12 complex I mutants from ~54,000 insertional mutants (Barbieri et al., 2011 and this study). Two *AMC* loci (*AMC9* and *AMC5)* encode for complex I subunits, verifying that the forward genetic screen yields *bona fide* complex I mutants. The other *amc* mutations remain yet-to-be determined and could map to any of the numerous genes encoding either complex I subunits or

biogenesis factors. Considering the number of proteins required for complex I biogenesis (Subrahmanian et al., 2016), it is clear our forward genetic screen is far from saturated. Screening for the *sid* phenotype appears to have only a 0.02% frequency of obtaining a *bona fide* complex I mutant. The use of a larger insertional mutant library, similar to the CLiP library generated by the Jonikas group (Zhang et al., 2014), could yield additional novel *AMC* loci. Unfortunately, in our experience, the conditions used for generating the CLiP mutants are more conducive for isolating photosynthetic-deficient mutants and less so for respiratory-deficient mutants. The Remacle group has devised a new method of screening for respiratory mutants that is based on the concerted contribution of the photosynthetic and respiratory systems to cellular ATP production (Massoz et al., 2017, 2015). They used the *pgrl1* mutant, defective for photosystem I cyclic electron transfer that is involved in ATP production in chloroplasts, as the background for generating respiratory mutants. Respiratory deficiency in the *pgrl1* background displayed an additional phenotype defined by decreased photosystem II efficiency, which was used as the basis to screen for complex I-deficient nuclear mutants (Massoz et al., 2017, 2015). Again, only three out of 3,059 transformants (0.09%) were identified as true complex I mutants from this screen. Future development of a screen to positively select or enrich for complex I mutants after mutagenesis might increase the success rate, yielding a larger number of nuclear mutants deficient for complex I.

Chlamydomonas has been previously used as a successful tool for studying human mitochondrial mutations. The L158P substitution in the mitochondrially encoded ND4 subunit, observed in one patient with chronic progressive external ophthalmoplegia (Pulkes, Liolitsa, Nelson, & Hanna, 2003), was shown to affect complex I activity but not assembly when reconstructed in *Chlamydomonas* (Larosa, Coosemans, Motte, Bonnefoy, & Remacle, 2012). In the second part of this study, we exploited the high degree of conservation *of Chlamydomonas* complex I nuclear-encoded subunits with their human counterparts (Cardol, 2011; Cardol et al., 2004) and demonstrated the efficacy of utilizing the newly uncovered *Chlamydomonas* nuclear mutants as a tool for defining the consequence of potentially pathogenic human mutations on complex I assembly and activity.

Both NUO5 (NDUFV2 in human) and NUOB10 (NDUFB10 in human) are highly conserved complex I subunits that have been identified as critical markers in human mitochondrial disorders (Benit et al., 2003; Cameron et al., 2015; Friederich et al., 2017; Nishioka et al., 2010; Zhang et al., 2009). NDUFV2 has been implicated in Alzheimer's disease, bipolar disorder, Parkinson's disease, and other pathologies. In this study, we tested a provisional mutation causing a lysine-to-arginine substitution in NDUFV2 and showed that it does not affect complex I activity or assembly. Indeed, comparative analyses of NDUFV2 orthologs revealed that an arginine residue is present at this position in *Thermus thermophilus*, *Arabidopsis*, and *Vitis vinifera* (Figure S5). As both lysine and arginine are positively charged amino acids, making the substitution of a conservative nature, it is likely this particular substitution is well-tolerated and does not elicit a change in complex I activity in *Chlamydomonas*. While complex I is a highly conserved enzyme in all eukaryotes, it is expected that some differences do exist between organisms regarding the point of entry of subunits during the assembly process (Vogel, Smeitink, & Nijtmans, 2007). Hence, we cannot rule out that the lack of an effect on complex I due to the lysine-to-arginine substitution is *Chlamydomonas*-specific. Three other SNPs in the *NDUFV2* gene resulting in amino acid substitutions of uncertain significance have been recently listed in the ClinVar database: P139T, M185V, and D190G. The P139T and M185V are especially interesting substitutions as these residues are very close to the cysteines involved in binding the Fe-S cluster (Figure S5). A future line of investigation could be to test the importance of these residues with our *nuo5*-null mutant.

The first patient reported with an isolated complex I disorder due to a mutation in the human nuclear *NDUFB10* gene presented an early-onset phenotype, characterized by prenatal cardiomyopathy along with metabolic acidosis and failure to thrive (Friederich et al., 2017). In concert with a compound heterozygous nonsense mutation, a missense mutation characterized by a cysteine-to-serine substitution of the first cysteine in the C-$(X)_{11}$-C motif resulted in decreased levels of complex I activity and increased accumulation of assembly intermediates in skeletal muscle, heart, and liver tissues (Friederich et al., 2017).

Recently, NDUFB10 was identified as an interacting partner of CHCHD4, a disulfide bond-forming enzyme, via affinity purification in both denaturing and native conditions, implying that NDUFB10 could be an in vivo target of CHCHD4 (Petrungaro et al., 2015). The CHCHD4-ALR import machinery (Mia40-Erv1 in yeast), also known as the mitochondrial IMS assembly system (MIA), functions by interacting with the cysteine residues of the substrate proteins and driving their import from the outer mitochondrial membrane into the IMS by coupling translocation with disulfide bond formation (Gabriel et al., 2007; Herrmann & Riemer, 2014). Canonical CHCHD4 substrates contain twin C-$(X)_3$-C or C-$(X)_9$-C motifs, whose cysteines form intramolecular disulfide bonds spanning the two motifs, enabling the formation of an anti-parallel helix–turn–helix structure (Herrmann & Riemer, 2014). The complex I subunits NDUFS5, NDUFB7, and NDUFA8 are canonical substrates of the CHCHD4-MIA system containing twin C-$(X)_9$-C motifs (Szklarczyk et al., 2011). Interestingly, the human NDUFB10 protein contains five cysteines in non-canonical motifs: a C-$(X)_6$-C motif, the C-$(X)_{11}$-C motif, and a fifth single cysteine (Figure S7). Pulse-chase experiments showed that cysteine thiols in NDUFB10 are no longer free after import into isolated human mitochondria and therefore presumed to be disulfide-linked (Friederich et al., 2017). It is expected that two disulfide bonds are formed in NDUFB10 upon import (Friederich et al., 2017). Although the identity of the disulfide bond-forming cysteines remains to be biochemically ascertained, single-particle electron cryo-microscopy of fungal, murine, bovine, and ovine complexes I model a disulfide bond between the cysteines within each motif of the NDUFB10 subunit (Agip et al., 2018; Letts, Fiedorczuk, Degliesposti, Skehel, & Sazanov, 2019; Parey et al., 2018; Zhu, Vinothkumar, & Hirst, 2016). As NDUFB10

does not have a canonical mitochondrial targeting sequence that is cleaved upon import (Hirst et al., 2003) and NDUFB10 sulfhydryl oxidation was shown to be CHCHD4-dependent, it was hypothesized to be imported to the IMS via the oxidative folding MIA mechanism (Friederich et al., 2017). In comparison with NDUFB10, the *Chlamydomonas* NUOB10 and other vascular plant orthologs contain only the C-$(X)_{11}$-C motif (Figure S7). If the cysteines are vital for mitochondrial import via the conserved oxidative folding mechanism, we should expect cysteine-to-serine substitutions of this motif to abolish NUOB10 import into the *Chlamydomonas* mitochondria and subsequent assembly into complex I. On the contrary, we observed that the single and double substitutions still allowed for incorporation of the NUOB10 variants into complex I, resulting in the accumulation of a mature holoenzyme (Figure 6). This finding is in accordance with the observations in the C107S NDUFB10 patient tissues, where complex I deficiency was not consistent across all tissues. For example, the skin fibroblasts appeared to express more of the C107S NDUFB10 variant than other tissues, enabling normal range of complex I activity (Friederich et al., 2017). These results indicate that the C107S substitution did not abolish NDUFB10's import into human mitochondria. Instead, the degree of complex I deficiency in different tissues was due to tissue-specific differential expression of this C107S variant. Our results further emphasize that both cysteine residues of the C-$(X)_{11}$-C motif are not strictly essential for NUOB10 import into the *Chlamydomonas* mitochondria.

One alternative explanation for the above-mentioned observations is that NUOB10/NDUFB10 is imported into the mitochondria in a CHCHD4-dependent but cysteine-independent manner. Such a phenomenon has been described for the IMS-localized mitochondrial protease Atp23 (Weckbecker, Longen, Riemer, & Herrmann, 2012), wherein the disulfide bonds are required for protein folding and stability, instead of mitochondrial import (Weckbecker et al., 2012). Atp23 is imported via hydrophobic interactions with CHCHD4, even in the absence of all cysteine residues. Interestingly, the yeast Atp23 contains ten cysteines, including one possible C-$(X)_{11}$-C motif similar to NDUFB10. All ten cysteines are involved in disulfide bond formation in the IMS, although the identity of the disulfide bond-forming cysteine residues remains unknown. A second possibility is that NUOB10 could be imported into the IMS via an alternative import mechanism independent of the MIA machinery, and is instead involved in post-import interaction with CHCHD4. For instance, it could be localized to the mitochondria by virtue of unknown internal targeting sequence(s) present in the protein, as is the case for BCS1, a factor required for complex III maturation (Stan et al., 2003). On the other hand, MICU1, another non-canonical substrate of the MIA machinery, contains a mitochondrial targeting sequence and is imported through a CHCHD4-independent transport. Post-import, CHCHD4 interacts with its substrate MICU1, catalyzing intermolecular disulfide bond formation, which enables the assembly of MICU1 into the mitochondrial calcium uniporter complex (Petrungaro et al., 2015).

Because the cysteine variants of NUOB10 are still incorporated into complex I, the subunit does not require disulfide bond formation at the C-$(X)_{11}$-C motif for import (Figure 6). However, significant decrease in rotenone-sensitive NADH: duroquinone oxidoreductase activity and lower accumulation of the mature complex is observed (Figure 6). Therefore, we propose that the cysteines, while not strictly required for mitochondrial import, may have roles in protein folding and stability, assembly into the membrane arm, and assisting the ubiquinone reduction, and/or proton-pumping capacity of complex I. The exact contribution of the C-$(X)_{11}$-C motif to complex I activity and assembly still remains to be determined.

In summary, we have successfully used *Chlamydomonas* for testing the impact of human pathogenic nuclear mutations on complex I assembly/activity, revealing the utility of a unicellular plant model as an experimental system of study for unraveling the molecular basis of complex I deficiencies. Even accounting for variations in the assembly process between *Chlamydomonas* and human complex I (Subrahmanian et al., 2016), it is reasonable to expect that analyzing nuclear pathogenic mutations in *Chlamydomonas* will provide insight into their consequence on complex I function. Our work opens up new avenues of exploration through a systematic approach, where substitutions of all conserved residues in complex I subunits, individually and in concert, could be methodically employed to document the functional importance of each residue in complex I assembly and activity.

ACKNOWLEDGMENTS

We thank Anniken Nilsen, Michael Subtelny, and Ruyuan Liu for their technical assistance. Thea A. Fatnes was a participant of the TRONDBUSS program. We are very grateful to Dr. Ty Johanness (University of Tulsa) for his kind gift of plasmids. This research was supported by a grant from the United Mitochondrial Disease Foundation (to PH).

CONFLICT OF INTEREST

The authors declare that they have no conflicts of interest with the contents of this article.

AUTHOR CONTRIBUTIONS

NS and PH contributed to the conception and design of the study, the acquisition, analysis, interpretation of the data, and writing of the manuscript. ADC contributed to acquisition, analysis or interpretation of the data, and critical reading of the manuscript. TAF acquired data.

REFERENCES

Agip, A. A., Blaza, J. N., Bridges, H. R., Viscomi, C., Rawson, S., Muench, S. P., & Hirst, J. (2018). Cryo-EM structures of complex I from mouse heart mitochondria in two biochemically defined states. *Nature Structural & Molecular Biology*, *25*, 548–556. https://doi.org/10.1038/s41594-018-0073-1

Ahlers, P. M., Garofano, A., Kerscher, S. J., & Brandt, U. (2000). Application of the obligate aerobic yeast *Yarrowia lipolytica* as a eucaryotic model to analyse Leigh syndrome mutations in the complex I core subunits PSST and TYKY. *Biochimica Et Biophysica Acta*, *1459*, 258–265. https://doi.org/10.1016/S0005-2728(00)00160-2

Banroques, J., Delahodde, A., & Jacq, C. (1986). A mitochondrial RNA maturase gene transferred to the yeast nucleus can control mitochondrial mRNA splicing. *Cell*, *46*, 837–844. https://doi.org/10.1016/0092-8674(86)90065-6

Barbieri, M. R., Larosa, V., Nouet, C., Subrahmanian, N., Remacle, C., & Hamel, P. P. (2011). A forward genetic screen identifies mutants deficient for mitochondrial complex I assembly in *Chlamydomonas reinhardtii*. *Genetics*, *188*, 349–358.

Bénit, P., Beugnot, R., Chretien, D., Giurgea, I., De Lonlay-Debeney, P., Issartel, J.-P., … Munnich, A. (2003). Mutant NDUFV2 subunit of mitochondrial complex I causes early onset hypertrophic cardiomyopathy and encephalopathy. *Human Mutation*, *21*, 582–586. https://doi.org/10.1002/humu.10225

Berrisford, J. M., Baradaran, R., & Sazanov, L. A. (2016). Structure of bacterial respiratory complex I. *Biochimica Et Biophysica Acta*, *1857*, 892–901.

Birrell, J. A., Morina, K., Bridges, H. R., Friedrich, T., & Hirst, J. (2013). Investigating the function of [2Fe-2S] cluster N1a, the off-pathway cluster in complex I, by manipulating its reduction potential. *The Biochemical Journal*, *456*, 139–146. https://doi.org/10.1042/BJ20130606

Cameron, J. M., MacKay, N., Feigenbaum, A., Tarnopolsky, M., Blaser, S., Robinson, B. H., & Schulze, A. (2015). Exome sequencing identifies complex I NDUFV2 mutations as a novel cause of Leigh syndrome. *European Journal of Paediatric Neurology*, *19*, 525–532. https://doi.org/10.1016/j.ejpn.2015.05.002

Cardol, P. (2011). Mitochondrial NADH: Ubiquinone oxidoreductase (complex I) in eukaryotes: A highly conserved subunit composition highlighted by mining of protein databases. *Biochimica Et Biophysica Acta*, *1807*, 1390–1397. https://doi.org/10.1016/j.bbabio.2011.06.015

Cardol, P., Boutaffala, L., Memmi, S., Devreese, B., Matagne, R. F., & Remacle, C. (2008). In *Chlamydomonas*, the loss of ND5 subunit prevents the assembly of whole mitochondrial complex I and leads to the formation of a low abundant 700 kDa subcomplex. *Biochimica Et Biophysica Acta*, *1777*, 388–396.

Cardol, P., Gloire, G., Havaux, M., Remacle, C., Matagne, R., & Franck, F. (2003). Photosynthesis and state transitions in mitochondrial mutants of *Chlamydomonas reinhardtii* affected in respiration. *Plant Physiology*, *133*, 2010–2020.

Cardol, P., Matagne, R. F., & Remacle, C. (2002). Impact of mutations affecting ND mitochondria-encoded subunits on the activity and assembly of complex I in *Chlamydomonas*. Implication for the structural organization of the enzyme. *Journal of Molecular Biology*, *319*, 1211–1221. https://doi.org/10.1016/S0022-2836(02)00407-2

Cardol, P., Vanrobaeys, F., Devreese, B., Van Beeumen, J., Matagne, R. F., & Remacle, C. (2004). Higher plant-like subunit composition of mitochondrial complex I from *Chlamydomonas reinhardtii*: 31 conserved components among eukaryotes. *Biochimica Et Biophysica Acta (BBA) - Bioenergetics*, *1658*, 212–224. https://doi.org/10.1016/j.bbabio.2004.06.001

Dent, R. M., Haglund, C. M., Chin, B. L., Kobayashi, M. C., & Niyogi, K. K. (2005). Functional genomics of eukaryotic photosynthesis using insertional mutagenesis of *Chlamydomonas reinhardtii*. *Plant Physiology*, *137*, 545–556.

Distelmaier, F., Koopman, W. J. H., van den Heuvel, L. P., Rodenburg, R. J., Mayatepek, E., Willems, P. H. G. M., & Smeitink, J. A. M. (2009). Mitochondrial complex I deficiency: From organelle dysfunction to clinical disease. *Brain*, *132*, 833–842. https://doi.org/10.1093/brain/awp058

Duarte, M., Schulte, U., Ushakova, A. V., & Videira, A. (2005). Neurospora strains harboring mitochondrial disease-associated mutations in iron-sulfur subunits of complex I. *Genetics*, *171*, 91–99. https://doi.org/10.1534/genetics.105.041517

Dujardin, G., Pajot, P., Groudinsky, O., & Slonimski, P. P. (1980). Long range control circuits within mitochondria and between nucleus and mitochondria. I. Methodology and phenomenology of suppressors. *Molecular and General Genetics*, *179*, 469–482.

Fiedorczuk, K., & Sazanov, L. A. (2018). Mammalian mitochondrial complex I structure and disease-causing mutations. *Trends in Cell Biology*, *28*, 835–867. https://doi.org/10.1016/j.tcb.2018.06.006

Friederich, M. W., Erdogan, A. J., Coughlin, C. R. II, Elos, M. T., Jiang, H., O'Rourke, C. P., … … J. (2017). Mutations in the accessory subunit NDUFB10 result in isolated complex I deficiency and illustrate the critical role of intermembrane space import for complex I holoenzyme assembly. *Human Molecular Genetics*, *26*, 702–716.

Gabriel, K., Milenkovic, D., Chacinska, A., Muller, J., Guiard, B., Pfanner, N., & Meisinger, C. (2007). Novel mitochondrial intermembrane space proteins as substrates of the MIA import pathway. *Journal of Molecular Biology*, *365*, 612–620. https://doi.org/10.1016/j.jmb.2006.10.038

Ghezzi, D., & Zeviani, M. (2018). Human diseases associated with defects in assembly of OXPHOS complexes. *Essays in Biochemistry*, *62*, 271–286. https://doi.org/10.1042/EBC20170099

Giachin, G., Bouverot, R., Acajjaoui, S., Pantalone, S., & Soler-Lopez, M. (2016). Dynamics of human mitochondrial complex I assembly: Implications for neurodegenerative diseases. *Frontiers in Molecular Biosciences*, *3*, 43. https://doi.org/10.3389/fmolb.2016.00043

Green, D. E., & Tzagoloff, A. (1966). The mitochondrial electron transfer chain. *Archives of Biochemistry and Biophysics*, *116*, 293–304. https://doi.org/10.1016/0003-9861(66)90036-1

Guerrero-Castillo, S., Baertling, F., Kownatzki, D., Wessels, H. J., Arnold, S., Brandt, U., & Nijtmans, L. (2017). The assembly pathway of mitochondrial respiratory chain complex I. *Cell Metabolism*, *25*, 128–139. https://doi.org/10.1016/j.cmet.2016.09.002

Harris, E. H. (1989). *The Chlamydomonas Sourcebook: A comprehensive guide to biology and laboratory use*. San Diego, CA: Academic Press.

Herrmann, J. M., & Riemer, J. (2014). Three approaches to one problem: Protein folding in the periplasm, the endoplasmic reticulum, and the intermembrane space. *Antioxidants & Redox Signaling*, *21*, 438–456. https://doi.org/10.1089/ars.2014.5841

Hirst, J. (2013). Mitochondrial complex I. *Annual Review of Biochemistry*, *82*, 551–575. https://doi.org/10.1146/annurev-biochem-070511-103700

Hirst, J., Carroll, J., Fearnley, I. M., Shannon, R. J., & Walker, J. E. (2003). The nuclear encoded subunits of complex I from bovine heart mitochondria. *Biochimica Et Biophysica Acta*, *1604*, 135–150.

Kerscher, S., Dröse, S., Zickermann, V., & Brandt, U. (2008). The three families of respiratory NADH dehydrogenases. In G. Schäfer, & H. Penefsky (Eds.), *Bioenergetics* (pp. 185–222). Berlin, Heidelberg: Springer.

Kerscher, S., Grgic, L., Garofano, A., & Brandt, U. (2004). Application of the yeast *Yarrowia lipolytica* as a model to analyse human pathogenic mutations in mitochondrial complex I (NADH: Ubiquinone oxidoreductase). *Biochimica Et Biophysica Acta*, *1659*, 197–205. https://doi.org/10.1016/j.bbabio.2004.07.006

Kmita, K., & Zickermann, V. (2013). Accessory subunits of mitochondrial complex I. *Biochemical Society Transactions*, *41*, 1272–1279. https://doi.org/10.1042/BST20130091

Koopman, W. J., Beyrath, J., Fung, C. W., Koene, S., Rodenburg, R. J., Willems, P. H., & Smeitink, J. A. (2016). Mitochondrial disorders in children: Toward development of small-molecule treatment strategies. *EMBO Molecular Medicine*, *8*, 311–327. https://doi.org/10.15252/emmm.201506131

Larosa, V., Coosemans, N., Motte, P., Bonnefoy, N., & Remacle, C. (2012). Reconstruction of a human mitochondrial complex I mutation in the unicellular green alga Chlamydomonas. *The Plant Journal*, *70*, 759–768.

Lasserre, J.-P., Dautant, A., Aiyar, R. S., Kucharczyk, R., Glatigny, A., Tribouillard-Tanvier, D., … di Rago, J.-P. (2015). Yeast as a system for modeling mitochondrial disease mechanisms and discovering therapies. *Disease Models & Mechanisms*, *8*, 509–526. https://doi.org/10.1242/dmm.020438

Lecler, R., Vigeolas, H., Emonds-Alt, B., Cardol, P., & Remacle, C. (2012). Characterization of an internal type-II NADH dehydrogenase from *Chlamydomonas reinhardtii* mitochondria. *Current Genetics*, *58*, 205–216. https://doi.org/10.1007/s00294-012-0378-2

Letts, J. A., Fiedorczuk, K., Degliesposti, G., Skehel, M., & Sazanov, L. A. (2019). Structures of respiratory supercomplex I+III2 reveal functional and conformational crosstalk. *Molecular Cell*, *75*, 1131–1146 e1136. https://doi.org/10.1016/j.molcel.2019.07.022

Liu, Y. G., Mitsukawa, N., Oosumi, T., & Whittier, R. F. (1995). Efficient isolation and mapping of *Arabidopsis thaliana* T-DNA insert junctions by thermal asymmetric interlaced PCR. *The Plant Journal*, *8*, 457–463. https://doi.org/10.1046/j.1365-313X.1995.08030457.x

Maclean, A. E., Kimonis, V. E., & Balk, J. (2018). Pathogenic mutations in NUBPL affect complex I activity and cold tolerance in the yeast model *Yarrowia lipolytica*. *Human Molecular Genetics*, *27*, 3697–3709. https://doi.org/10.1093/hmg/ddy247

Massoz, S., Hanikenne, M., Bailleul, B., Coosemans, N., Radoux, M., Miranda-Astudillo, H., ..., ... C. (2017). In vivo chlorophyll fluorescence screening allows the isolation of a Chlamydomonas mutant defective for NDUFAF3, an assembly factor involved in mitochondrial complex I assembly. *The Plant Journal*, *92*, 584–595.

Massoz, S., Larosa, V., Horrion, B., Matagne, R. F., Remacle, C., & Cardol, P. (2015). Isolation of *Chlamydomonas reinhardtii* mutants with altered mitochondrial respiration by chlorophyll fluorescence measurement. *Journal of Biotechnology*, *215*, 27–34. https://doi.org/10.1016/j.jbiotec.2015.05.009

Mitchell, A. L., Elson, J. L., Howell, N., Taylor, R. W., & Turnbull, D. M. (2006). Sequence variation in mitochondrial complex I genes: Mutation or polymorphism? *Journal of Medical Genetics*, *43*, 175–179.

Mitchell, P. (1961). Coupling of phosphorylation to electron and hydrogen transfer by a chemi-osmotic type of mechanism. *Nature*, *191*, 144–148. https://doi.org/10.1038/191144a0

Nishioka, K., Vilariño-Güell, C., Cobb, S. A., Kachergus, J. M., Ross, O. A., Hentati, E., ... Farrer, M. J. (2010). Genetic variation of the mitochondrial complex I subunit NDUFV2 and Parkinson's disease. *Parkinsonism & Related Disorders*, *16*, 686–687. https://doi.org/10.1016/j.parkreldis.2010.09.007

Pagniez-Mammeri, H., Loublier, S., Legrand, A., Benit, P., Rustin, P., & Slama, A. (2012). Mitochondrial complex I deficiency of nuclear origin I. Structural Genes. *Molecular Genetics and Metabolism*, *105*, 163–172. https://doi.org/10.1016/j.ymgme.2011.11.188

Parey, K., Brandt, U., Xie, H., Mills, D. J., Siegmund, K., Vonck, J., ... Zickermann, V. (2018). Cryo-EM structure of respiratory complex I at work. *Elife*, *7*, e39213. https://doi.org/10.7554/eLife.39213.001

Petrungaro, C., Zimmermann, K. M., Kuttner, V., Fischer, M., Dengjel, J., Bogeski, I., & Riemer, J. (2015). The Ca(2+)-dependent release of the Mia40-induced MICU1-MICU2 dimer from MCU regulates mitochondrial Ca(2+) uptake. *Cell Metabolism*, *22*, 721–733. https://doi.org/10.1016/j.cmet.2015.08.019

Pulkes, T., Liolitsa, D., Nelson, I. P., & Hanna, M. G. (2003). Classical mitochondrial phenotypes without mtDNA mutations. *Neurology*, *61*, 1144–1147.

Purton, S., & Rochaix, J. D. (1994). Complementation of a *Chlamydomonas reinhardtii* mutant using a genomic cosmid library. *Plant Molecular Biology*, *24*, 533–537.

Remacle, C., Barbieri, M. R., Cardol, P., & Hamel, P. P. (2008). Eukaryotic complex I: Functional diversity and experimental systems to unravel the assembly process. *Molecular Genetics and Genomics*, *280*, 93–110.

Remacle, C., Baurain, D., Cardol, P., & Matagne, R. F. (2001b). Mutants of *Chlamydomonas reinhardt*ii deficient in mitochondrial complex I: Characterization of two mutations affecting the *nd1* coding sequence. *Genetics*, *158*, 1051–1060.

Remacle, C., Cardol, P., Coosemans, N., Gaisne, M., & Bonnefoy, N. (2006). High-efficiency biolistic transformation of *Chlamydomonas* mitochondria can be used to insert mutations in complex I genes. *Proceedings of the National Academy of Sciences of the United States of America*, *103*, 4771–4776. https://doi.org/10.1073/pnas.0509501103

Remacle, C., Duby, F., Cardol, P., & Matagne, R. F. (2001a). Mutations inactivating mitochondrial genes in *Chlamydomonas reinhardtii*. *Biochemical Society Transactions*, *29*, 442–446. https://doi.org/10.1042/bst0290442

Remacle, C., Gloire, G., Cardol, P., & Matagne, R. F. (2004). Impact of a mutation in the mitochondrial LSU rRNA gene from *Chlamydomonas reinhardtii* on the activity and the assembly of respiratory-chain complexes. *Current Genetics*, *45*, 323–330. https://doi.org/10.1007/s00294-004-0490-z

Remacle, C., Hamel, P., Larosa, V., Subrahmanian, N., & Cardol, P. (2012).A structural perspective on complex I.In L. Sazanov (Ed.), *Complexes I in the green lineage* (pp. 219–244). Springer.

Rodenburg, R. J. (2016). Mitochondrial complex I-linked disease. *Biochimica Et Biophysica Acta*, *1857*, 938–945. https://doi.org/10.1016/j.bbabio.2016.02.012

Saada, A., Edvardson, S., Rapoport, M., Shaag, A., Amry, K., Miller, C., ... Elpeleg, O. (2008). C6ORF66 is an assembly factor of mitochondrial complex I. *American Journal of Human Genetics*, *82*, 32–38. https://doi.org/10.1016/j.ajhg.2007.08.003

Salinas, T., Larosa, V., Cardol, P., Marechal-Drouard, L., & Remacle, C. (2014). Respiratory-deficient mutants of the unicellular green alga Chlamydomonas: A review. *Biochimie*, *100*, 207–218. https://doi.org/10.1016/j.biochi.2013.10.006

Schägger, H., & von Jagow, G. (1991). Blue native electrophoresis for isolation of membrane protein complexes in enzymatically active form. *Analytical Biochemistry*, *199*, 223–231.

Sharma, L. K., Lu, J., & Bai, Y. (2009). Mitochondrial respiratory complex I: Structure, function and implication in human diseases. *Current Medicinal Chemistry*, *16*, 1266–1277.

Shimogawara, K., Fujiwara, S., Grossman, A., & Usuda, H. (1998). High-efficiency transformation of *Chlamydomonas reinhardtii* by electroporation. *Genetics*, *148*, 1821–1828.

Shoubridge, E. A. (2001). Nuclear genetic defects of oxidative phosphorylation. *Human Molecular Genetics*, *10*, 2277–2284. https://doi.org/10.1093/hmg/10.20.2277

Silhavy, T. J., Berman, M. L., & Enquist, L. W. (1984). *Experiments with gene fusions*. Plainview, NY: Cold Spring Harbor Laboratory Press.

Sokalingam, S., Raghunathan, G., Soundrarajan, N., & Lee, S. G. (2012). A study on the effect of surface lysine to arginine mutagenesis on protein stability and structure using green fluorescent protein. *PLoS ONE*, *7*, e40410. https://doi.org/10.1371/journal.pone.0040410

Stan, T., Brix, J., Schneider-Mergener, J., Pfanner, N., Neupert, W., & Rapaport, D. (2003). Mitochondrial protein import: Recognition of internal import signals of BCS1 by the TOM complex. *Molecular and Cellular Biology*, *23*, 2239–2250. https://doi.org/10.1128/MCB.23.7.2239-2250.2003

Stroud, D. A., Surgenor, E. E., Formosa, L. E., Reljic, B., Frazier, A. E., Dibley, M. G., ... Ryan, M. T. (2016). Accessory subunits are integral for assembly and function of human mitochondrial complex I. *Nature*, *538*, 123–126. https://doi.org/10.1038/nature19754

Subrahmanian, N., Remacle, C., & Hamel, P. P. (2016). Plant mitochondrial Complex I composition and assembly: A review. *Biochimica Et Biophysica Acta*, *1857*, 1001–1014. https://doi.org/10.1016/j.bbabio.2016.01.009

Szklarczyk, R., Wanschers, B. F., Nabuurs, S. B., Nouws, J., Nijtmans, L. G., & Huynen, M. A. (2011). NDUFB7 and NDUFA8 are located at the intermembrane surface of complex I. *FEBS Letters*, *585*, 737–743. https://doi.org/10.1016/j.febslet.2011.01.046

Vinothkumar, K. R., Zhu, J., & Hirst, J. (2014). Architecture of mammalian respiratory complex I. *Nature*, *515*, 80–84. https://doi.org/10.1038/nature13686

Vogel, R. O., Smeitink, J. A., & Nijtmans, L. G. (2007). Human mitochondrial complex I assembly: A dynamic and versatile process. *Biochimica Et Biophysica Acta*, *1767*, 1215–1227. https://doi.org/10.1016/j.bbabio.2007.07.008

Weckbecker, D., Longen, S., Riemer, J., & Herrmann, J. M. (2012). Atp23 biogenesis reveals a chaperone-like folding activity of Mia40 in the IMS of mitochondria. *EMBO Journal*, *31*, 4348–4358. https://doi.org/10.1038/emboj.2012.263

Zhang, J., Li, X., Wang, Y., Ji, J., Yang, F., Feng, G., … He, G. (2009). Association study on the mitochondrial gene NDUFV2 and bipolar disorder in the Chinese Han population. *Journal of Neural Transmission*, *116*, 357–361. https://doi.org/10.1007/s00702-009-0185-1

Zhang, R., Patena, W., Armbruster, U., Gang, S. S., Blum, S. R., & Jonikas, M. C. (2014). High-throughput genotyping of green algal mutants reveals random distribution of mutagenic insertion sites and endonucleolytic cleavage of transforming DNA. *The Plant Cell*, *26*, 1398–1409. https://doi.org/10.1105/tpc.114.124099

Zhu, J., King, M. S., Yu, M., Klipcan, L., Leslie, A. G. W., & Hirst, J. (2015a). Structure of subcomplex Iβ of mammalian respiratory complex I leads to new supernumerary subunit assignments. *Proceedings of the National Academy of Sciences of the United States of America*, *112*, 12087–12092. https://doi.org/10.1073/pnas.1510577112

Zhu, J., King, M. S., Yu, M., Klipcan, L., Leslie, A. G., & Hirst, J. (2015b). Structure of subcomplex Ibeta of mammalian respiratory complex I leads to new supernumerary subunit assignments. *Proceedings of the National Academy of Sciences of the United States of America*, *112*, 12087–12092.

Zhu, J., Vinothkumar, K. R., & Hirst, J. (2016). Structure of mammalian respiratory complex I. *Nature*, *536*, 354–358. https://doi.org/10.1038/nature19095

SUPPORTING INFORMATION

Additional supporting information may be found online in the Supporting Information section.

How to cite this article: Subrahmanian N, Castonguay AD, Fatnes TA, Hamel PP. *Chlamydomonas reinhardtii* as a plant model system to study mitochondrial complex I dysfunction. *Plant Direct*. 2020;4:1–16. https://doi.org/10.1002/pld3.200

Chlamydomonas reinhardtii as a plant model system to study mitochondrial complex I dysfunction

Nitya Subrahmanian, Andrew David Castonguay, Thea Aspelund Fatnes, and Patrice Paul Hamel [*].

Nitya Subrahmanian

Department of Molecular Genetics, The Ohio State University, Columbus, Ohio, USA.

Plant Cellular and Molecular Biology Graduate Program, The Ohio State University, Columbus, Ohio, USA.

Email: subrahmanian.1@buckeyemail.osu.edu

Andrew David Castonguay

Department of Molecular Genetics, The Ohio State University, Columbus, Ohio, USA.

Molecular Genetics Graduate Program, The Ohio State University, Columbus, Ohio, USA.

Email: castonguay.3@buckeyemail.osu.edu

Thea Aspelund Fatnes

Department of Molecular Genetics, The Ohio State University, Columbus, Ohio, USA.

Present address: Fürst Medical Laboratory, Soren Bulls Vei 25, 1051 Oslo, Norway.

Email: t.aspelund.f@gmail.com

Patrice Paul Hamel

Department of Molecular Genetics, Department of Biological Chemistry and Pharmacology, The Ohio State University, Columbus, Ohio, USA.

[*] To whom correspondence should be addressed: Patrice P. Hamel, Room 582 Aronoff Laboratory, 318 W. 12th Ave, Columbus, Ohio 43210, USA. Tel.: +1 614-292-3817; Fax: +1 614-292-6345;

E-mail: hamel.16@osu.edu.

List of Supplemental Information

Supplemental Methods:

Supplemental Figures:

Supplemental Figure S9. The FLAG-tagged variants of NUOB10 are produced in the *amc5* mutant.

Supplemental Tables:

Supplemental Table S1. Sequence of primers used in this study.

Supplemental Table S2. Primers used for recombinant cloning.

Supplemental Table S3. Method of plasmid construction.

Supplemental Table S4. Summary of biolistic transformation.

Supplemental Methods

Supplemental Method S1: Insertional mutagenesis and phenotypic screening of complex I mutants

Transformation of 4C$^-$ (*mt*$^-$; *arg7-8*) [CC-5590] strain was conducted after autolysine treatment by electroporation (Shimogawara *et al.*, 1998). The strain was grown in liquid TARG medium for 2-3 days until exponential growth (3 – 6 x 10^6 cells. mL^{-1}). For each transformation, 2.5 x 10^7 cells were electroporated at 1.3 kV and 10 µF with 100 ng of hygromycin B resistance cassette (iHyg3) and 20 µg of herring sperm DNA. The iHyg3 cassette consists of the *APHVII* gene with an *RBCS2* intron, under the control of the β2 tubulin-encoding gene (*TUB2*) promoter and the *RBCS2* terminator (Figure S4A). This cassette was amplified from the pHyg3 plasmid (Berthold *et al.*, 2002) using the primers: APH7-F and APH7-R (Table S1). The transformants were selected on TARG+HyB solid medium. Candidate complex I-deficient mutants were identified by scoring for the SID phenotype (Barbieri *et al.*, 2011). Hygromycin B resistant (HyB^R) colonies, which appeared after 10 days of incubation, were transferred into 400 µl of TARG + HyB liquid medium in 96-well plates, each well containing a single colony. The 96-well plate was incubated for five days at 25°C in continuous light at 50 µmol m^{-2} s^{-1}. The liquid cultures were then replica-plated onto two solid TARG media, incubated in the light and dark for five days. Transformants with a SID phenotype were selected and sub-cloned three times to obtain a single colony prior to further analysis. The *amc* mutant strains isolated in this study and their corresponding *Chlamydomonas Resource Center* reference numbers are as follows: *amc8 (1H5)* [CC-5600], *amc9 (41D9)* [CC-5601], *amc10 (12C)* [CC-5606], *amc11 (10G11)* [CC-5608], *amc12 (6E9)* [CC-5611], *amc13 (4C3)* [CC-5612], and *amc13(16)* [CC-5613].

Supplemental Method S2: Genetic analysis of the amc mutants

Genetic crosses were done as in (Harris, 1989) with some modifications. Vegetative cells were resuspended in TAP liquid medium lacking nitrogen (TAP-N), at 25°C in low light at .5-1 µmol m^{-2} s^{-1}, with shaking for a minimum of 5 hr. Equal volumes of the resultant gametes (of opposite mating types) were mixed and incubated in 50 µmol m^{-2} s^{-1} light at 25°C overnight to accomplish mating. In some cases, 10 mM dibutyryl-cAMP (WJ Pharmaceuticals, 100862) and/or 1 mM IBMX (Sigma, 15879-1G) were added to the mixture to stimulate mating. The mixture was plated on TAP-N solid medium (containing 3% (w/v) select agar) and incubated in high light at 25°C for 5 days, to allow the maturation of meiotic zygotes. Meiosis was induced by transferring the zygotes on TARG solid medium, in high light at 25°C,

for at least 12 – 16 hr. The meiotic progeny was obtained through bulk germination or tetrad dissection of zygotes.

In this study, the background strains 141 (*mt*$^{+}$*; arg9-2*), CC-125 (137C^{+}), or 1' (*mt*$^{+}$) were crossed with the original *amc* mutants. Meiotic *amc* progeny derived from these crosses were also used for experimentation. Especially for *amc10* and *amc13*, their meiotic derivatives *amc10(12C)* and *amc13(16)* were used for analyses. For constructing *amc/+* diploids, the *amc* mutants (*mt*$^{-}$; *amc*; *APHVII*; *arg7-8*) were crossed with CC-125 and the mating mixture was directly plated on selective medium (TAP + HyB). Individual diploids or meiotic progeny were subcloned to a single colony and their mating type was determined by diagnostic PCR (Werner & Mergenhagen, 1998).

Supplemental Method S3: Ten-fold dilution series and growth curve analysis

The SID phenotype was tested by ten-fold dilution series as follows. One loop of cells grown on solid TARG plates (for 3-5 days) was resuspended in 500 µl of liquid TARG medium. The cell density was measured spectrophotometrically at 750 nm and normalized to an OD_{750} = 2.0 by dilution. This normalized suspension was used as the starting material [1] for making five serial ten-fold dilutions [10^{-1}, 10^{-2}, 10^{-3}, 10^{-4}, and 10^{-5}]. A volume of 8 µl for each dilution was plated on solid TARG plates. For scoring the SID phenotype, two plates were prepared simultaneously and incubated at 25°C, one in continuous light and another in continuous dark, for at least 7 days. The light-incubated plate served as a control for confirming equal cell density amongst multiple strains.

To determine the generation time, liquid cultures were inoculated with a starting cell density of 10^5 cells. mL^{-1} in 50 mL TARG medium. Growth in liquid culture was observed by evaluating cell density at A_{750}. Measurements were taken every 8 hr over a period of 10 days. For each strain, three biological replicates were inoculated in continuous light at 25 µmol m^{-2} s^{-1} or in continuous darkness. Growth rate µ was calculated as $3.3*[\log_{10}N - \log_{10}N_0] / (t_N-t_0)$, where N is the final cell density at time t_N and N_0 is the initial cell density at time t_0. The generation time was calculated as 1/ µ (Harris, 1989, Kropat *et al.*, 2011).

The time periods used for calculating doubling times are as follows: For wild-type (4C^{-}) and [*amc9*; *NUO5*] strains in the light t_N = 86 hr and t_0 = 26 hr, and in the dark t_N = 110 hr and t_0 = 38 hr; for the *amc9* strain in the light t_N = 110 hr and t_0 = 38 hr, and in the dark t_N = 170 hr and t_0 = 86 hr; for wild-type (3A^{+}) in the light t_N = 96 hr and t_0 = 24 hr; for wild-type in the dark t_N = 120 hr and t_0 = 36 hr; for *amc5* in the

light t_N = 85 hr and t_0 = 37 hr; for *amc5* in the dark t_N = 123 hr and t_0 = 49 hr; for [*amc5*; *NUOB10*] in the light t_N = 85 hr and t_0 = 37 hr and for [*amc5*; *NUOB10*] in the dark t_N = 123 hr and t_0 = 37 hr.

Supplemental Method S4: Nucleic acid extraction, diagnostic PCRs and real-time qPCRs

Genomic DNA was extracted from *Chlamydomonas* by the phenol-chloroform method with some modifications (Sambrook *et al.*, 1989). One or two loops of cells, grown for two to three days in continuous light at 50 µmol m^{-2} s^{-1} on TARG solid medium, was harvested and resuspended in buffer (10 mM Tris-HCl, pH 8, 10 mM EDTA, 10 mM NaCl, 15% (w/v) glycerol). Cells were lysed by sonication for 5 s at 9 W output. Proteins were degraded by treatment with 100 µg proteinase K (Invitrogen, 25530049) and the extract was incubated at 55 ºC for one hour. RNA was degraded with 50 µg RNase A (Amresco, 0675-250mg). Nucleic acids were extracted twice by phenol-chloroform and DNA was precipitated by adding 2.2 volumes of ethanol and .1 volume of 3 M Na acetate pH 5.5.

The sequences of primers used for diagnostic PCR are shown in Table S1. For diagnostic PCR analysis, GoTaq Polymerase (Promega, M3008) was used as recommended by the manufacturer. To enhance the amplification of GC-rich regions, 2.5% (v/v) DMSO was used in each reaction in addition to a denaturation temperature of 98 ºC (instead of 95 ºC). For sequencing analyses, PCR products were gel-purified using the NucleoSpin Gel Extraction Kit (Machery Nagel, 740609.25) as per the manufacturer's instructions. The purified PCR product was then cloned into pGEM-T Easy Vector Systems (Promega, A1360) and then sequenced with T7 and SP6 primers flanking the cloning site.

For real-time quantitative PCR, RNA was prepared as in (Newman *et al.*, 1990). RNA was extracted from 2 x 10^8 cells grown in liquid culture. Nucleic acids were extracted twice with equal volume of phenol-chloroform (pH 5.0) and RNA was precipitated after overnight incubation at -20°C with 1/3rd volume of 8 M LiCl. Eight micrograms of RNA were treated with RQ1 RNase-free DNase I (Promega, M6101). Reverse transcription was achieved with 400 units of M-MLV Reverse transcriptase (Life Technologies, 28025-013) using one microgram of Random Hexamers (Promega, C1181), following the manufacturer's protocol. Amount of cDNA equivalent to 50 ng or 100 ng of total input RNA was used as template for qPCR using SensiMix (Bioline, QT-650-05) on a Mastercycler ep gradientS realplex thermocycler (Eppendorf). The sequences of primers used in qPCR are detailed in Table S1. The primer pairs NUO5E2L2 / NUO5E3R and NUOB10E4L / NUOB10E4R were used to amplify *NUO5* and *NUOB10* mRNA, respectively. The transcript abundance of the housekeeping genes *CBLP* (*Cre13.g599400*) and

EIF1A (*Cre02.g103550*) were determined using the primers CBLP-F / CBLP-R and EIF1A-Fw / EIF1A-Rev, respectively. Transcript abundance of E3 ubiquitin ligase *UBI* (*Cre03.g159200*) was determined by using primers Ubiupper / Ubilower and *TUA2* (*Cre04.g216850*) using Tub-F / Tub-R (de Montaigu *et al.*, 2011). Primer efficiencies for primers binding to *NUO5, NUOB10, TUA2, CBLP, UBI*, and *EIF1A*, determined by calibration curves, were 95%, 100%, 100%, 108%, 93%, and 99.8%, respectively. The target transcript was normalized to three reference transcripts by the Livak $2^{-\Delta\Delta Ct}$ method (Livak & Schmittgen, 2001). Three independent biological replicates were performed, each analyzed using two technical replicates. The qPCR reactions were denatured at 98 ºC for 15 s, annealed at 60 ºC for 20 s and extended at 72 ºC for 20 s. Relative fold change was determined by normalizing to the average of the isogenic wild-type strain. Results are represented as percentage of wild-type strain.

Supplemental Method S5: Plasmid construction

Plasmids expressing the *NUO5* and *NUOB10* wild-type and mutant genes were generated by recombination-based cloning in yeast. The pRS426-ble plasmid, containing three markers allowing for selection in algae, yeast, and bacteria, was used as the vector (Noor-Mohammadi *et al.*, 2014). It contains the *ble* gene conferring zeocin resistance for selection in *Chlamydomonas*, the *URA3* gene for selection in *S. cerevisiae*, and the *bla* gene conferring ampicillin resistance in *E. coli*. The pRS426-ble plasmid was linearized with *Not*I and *Ale*I (pB-NA). The *NUO5* and the *NUOB10* genes were cloned between the *Not*I and *Ale*I sites in pRS426-ble. The *NUO5* and *NUOB10* genes were expressed under their putative native promoters by including the entire intergenic region upstream of each gene (1220 bp and 1075 bp for *NUO5* and *NUOB10*, respectively). Each gene, including its promoter region, was amplified from purified genomic DNA using Velocity DNA Polymerase (Bioline, BIO21098) as consecutive overlapping fragments (Table S2). The sequence corresponding to the C-terminal FLAG-tag and site-directed mutations were introduced by PCR with appropriately designed primers (Table S2). The overlapping PCR fragments and linearized vector (pB-NA) were assembled via *in vivo* molecular recombination in yeast (Table S3). The *S. cerevisiae* strain CW04 (Banroques *et al.*, 1986) was used for recombination. Two hundred nanograms of each linear fragment was introduced into the strain by the one-step transformation method (Chen *et al.*, 1992, Saint-Georges *et al.*, 2002) and cells containing the recombinant clones were selected based on uracil prototrophy. Successful recombinants were identified based on diagnostic PCR and restriction digestion, verified by sequencing, and introduced into the respective *Chlamydomonas* strains by biolistics. However, the *ble* selection in *Chlamydomonas* was not successful as it led to the emergence of spontaneous zeocin-resistant colonies in which the transforming DNA was absent. Hence,

the *ble* selection marker was substituted with the *APHVII* selection marker (iHyg3) conferring HyB resistance (for the *NUOB10* clones) or *APHVIII* selection marker (iPm) conferring Pm resistance (for the *NUO5* clones). The *ble* marker (1.18 kb) was excised from each plasmid with *Eco*RI and *Not*I restriction enzymes. The iHyg3 and iPm markers were amplified from the plasmids pHyg3 and pSL18 (Berthold *et al.*, 2002, Depege *et al.*, 2003), respectively, using Velocity DNA Polymerase (Bioline, BIO21098) with primers including a 25 bp overlap with the digested vector (Table S2). Cloning of the new selection markers were achieved using the In-Fusion HD Cloning Kit (Clontech, 639648) according to the manufacturer's protocol (Table S3). The recombinant clones finally used for *Chlamydomonas* transformation are: pRS426-iPm-NUO5-WT-FLAG and pRS426-iPm-NUO5-K230R-FLAG for the *amc9* strain (41D9); pRS426-iHyg3-NUOB10-WT-FLAG, pRS426-iHyg3-NUOB10-C79S-FLAG, pRS426-iHyg3-NUOB10-C91S-FLAG, and pRS426-iHyg3-NUOB10-C79SC91S-FLAG for the *amc5* strain (87D3) (as detailed in Tables S3 and S4).

Supplemental Method S6: Complex II+III and Complex IV enzymatic assays

Activity assays were conducted on crude membrane extracts that were prepared as described in Materials and Methods section. Complex II+III activity assay was conducted in the presence of 20.25 mM succinate (Acros organics, 158751000), 1 mM KCN (FisherScientific, P223I-100) and 56 µM equine heart cytochrome *c* (Sigma, 2506-500mg). The activity was determined as the rate of cytochrome *c* reduction and measured spectrophotometrically at $A_{550.}$ Complex II+III activity was calculated using molar extinction coefficient for cytochrome *c* at $\Delta\varepsilon_{550nm}$ = 19.6 mM^{-1} cm^{-1}, in the absence and presence of complex III-specific inhibitor myxothiazol (3 µM) (Sigma, T5580). Complex IV activity assay was conducted in the presence of 1% Triton X-100 and 56 µM reduced cytochrome *c*. Cytochrome *c* was reduced with two times the amount of sodium dithionite and purified with a PD10-desalting column with Sephadex G-25 resin (GE Lifesciences, 17085101) according to the manufacturer's protocol. Complex IV activity was calculated using molar extinction coefficient for cytochrome *c* at $\Delta\varepsilon_{550nm}$ = 19.6 mM^{-1} cm^{-1}, in the absence and presence of complex IV inhibitor KCN (1 mM).

Supplemental Method S7: Immunoblotting analysis

BN-PAGE was completed as described in Materials and Methods section. For SDS-PAGE, 10 µg of crude membrane proteins was separated by 12.5% acrylamide gel and immunoblotting was performed according to established protocols (Sambrook *et al.*, 1989). The separated proteins were electro-blotted onto PVDF

membranes and custom-made rabbit polyclonal antibodies specific for *Chlamydomonas* complex I subunits (from Genescript, as described in (Barbieri *et al.*, 2011)), were used. Membranes with electroblotted proteins separated in BN-PAGE gels were probed overnight at 4°C with 1:3000 diluted α-51 kDa, a polyclonal antibody that detects the soluble arm 51 kDa subunit. Membranes containing proteins resolved by SDS-PAGE immunoblots were probed at room temperature for 3 hr with 1:3000 diluted α-51 kDa, 1: 3000 diluted α-49 kDa, 1:2000 diluted α-TYKY and for 1 hr with 1:12,000 diluted α-cytochrome *f* (Dreyfuss et al., 2003). For rabbit polyclonal antibodies, a HRP-conjugated anti-rabbit Goat IgG (Biorad, 170-6515) at 1:10,000 dilution was used as the secondary antibody. For detecting the FLAG-tagged proteins, membranes were incubated with monoclonal anti-FLAG antibody (Sigma, F1804) at 1:5000 dilution overnight at 4°C followed by a HRP-conjugated anti-mouse Goat IgG (Pierce 18584_3) at a dilution of 1:2,500 as the secondary antibody. Intensity of bands in immunoblots were quantified using ImageJ (Schneider *et al.*, 2012).

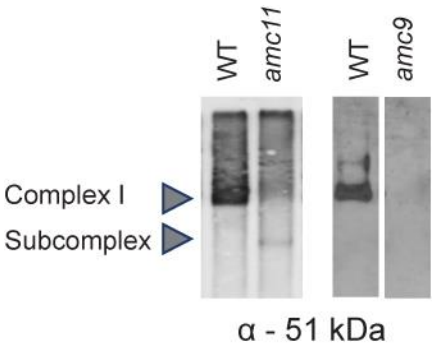

Supplemental Figure S1. Additional Blue-Native PAGE immunoblotting analyses.

Blue-Native PAGE followed by immunoblotting was conducted on crude membrane extracts using a polyclonal antibody to detect the 51 kDa subunit of complex I. The white vertical line between the lanes of WT and *amc9* denotes the assembly of lanes from the same blot.

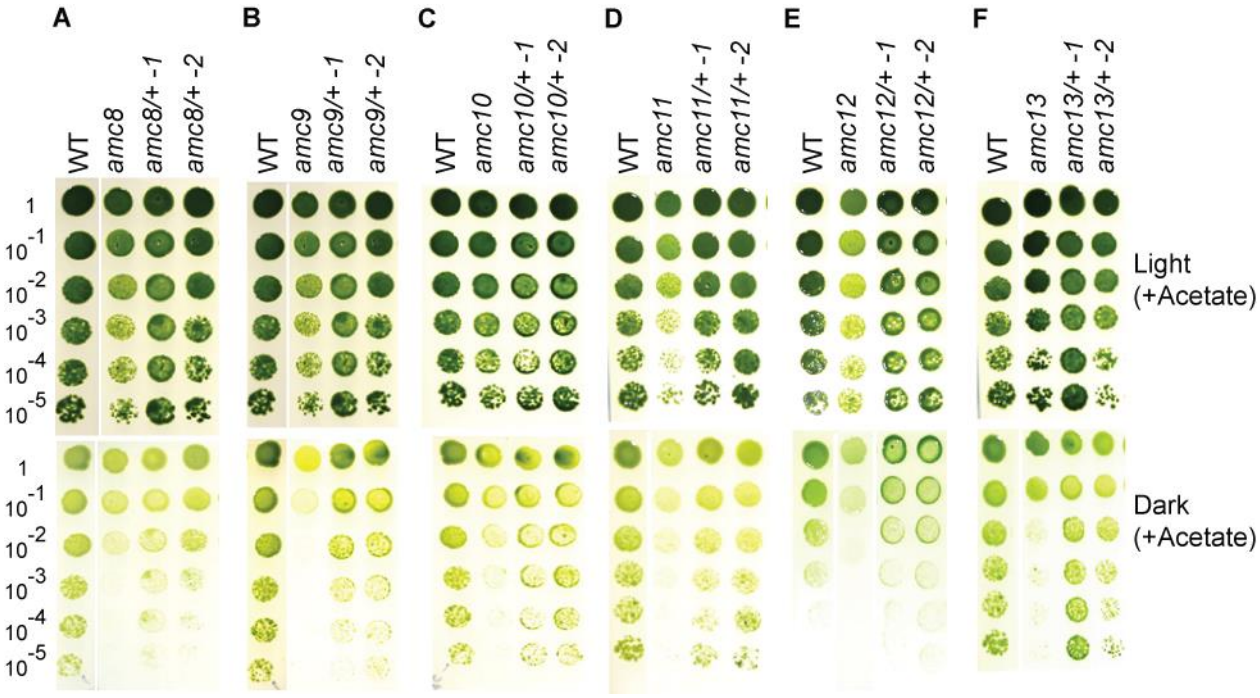

Supplemental Figure S2. The *amc8* to *amc13* mutations are recessive.

To test if the *amc* mutations causing the complex I-deficient phenotype are recessive or dominant with respect to the wild-type allele, heterozygous diploids (*amc*/+) were constructed by crossing *amc* mutants with a wild-type strain as described in Method S2. Two independent diploids from each cross were tested for growth in the dark by ten-fold dilution series. The dilution series were plated on acetate-containing medium and incubated in the light or dark for 10 days. The heterozygous *amc*/+ diploids were restored for growth in the dark, thereby indicating that all the *amc* mutations are recessive. White vertical lines indicate pictures of strains grown from the same plate and assembled for the display in the figure. The growth of the following diploids is depicted in panels A-F wherein WT ($4C^-$) and the respective *amc* mutants, used for constructing the diploids, were used as controls: A, *amc8*/+; B, *amc9*/+; C, *amc10*/+; D, *amc11*/+; E, *amc12*/+; F, *amc13*/+.

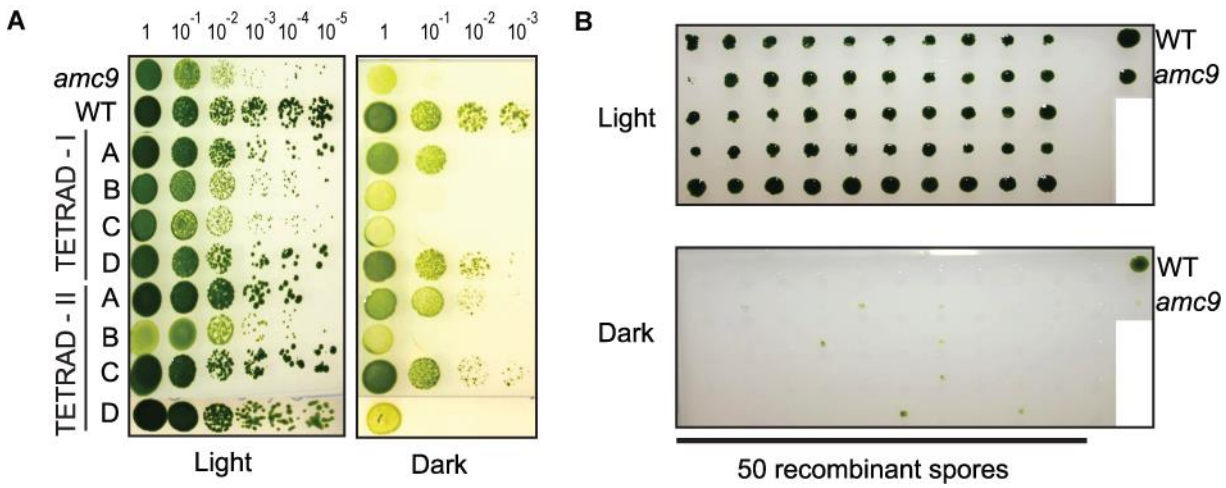

Supplemental Figure S3. The *amc9* mutation is linked to the insertional cassette.

Meiotic zygotes were obtained by crossing the complex I proficient strain 141 (mt^+; *arg9*-2) with the complex I-deficient *amc9* (*3*$^-$) strain (mt^-; *nuo5::APHVII*). The meiotic zygotes, obtained from the same genetic cross, were used for both tetrad dissection (A) and bulk germination (B). (A) The growth phenotype of two out of seven tetrads dissected from the above-mentioned cross is shown here by ten-fold dilution series. The dilutions were plated on acetate-containing medium and incubated in the light and in the dark for 15 days. The WT strain and the *amc9* strain shown here are the original parental strains. (B) Fifty recombinant hygromycin B resistant progeny, were analyzed from bulk germination of meiotic zygotes. The progeny were replica-plated on TARG solid medium in the light or dark and the growth phenotype was scored after 15 days of incubation. The WT and *amc9* strains shown here are 4C$^-$ and *amc9 (41D9)*, respectively. Out of 50 antibiotic-resistant meiotic progeny that were tested, all of them displayed a SID phenotype confirming that the *amc9* mutation is tightly linked to the insertional cassette.

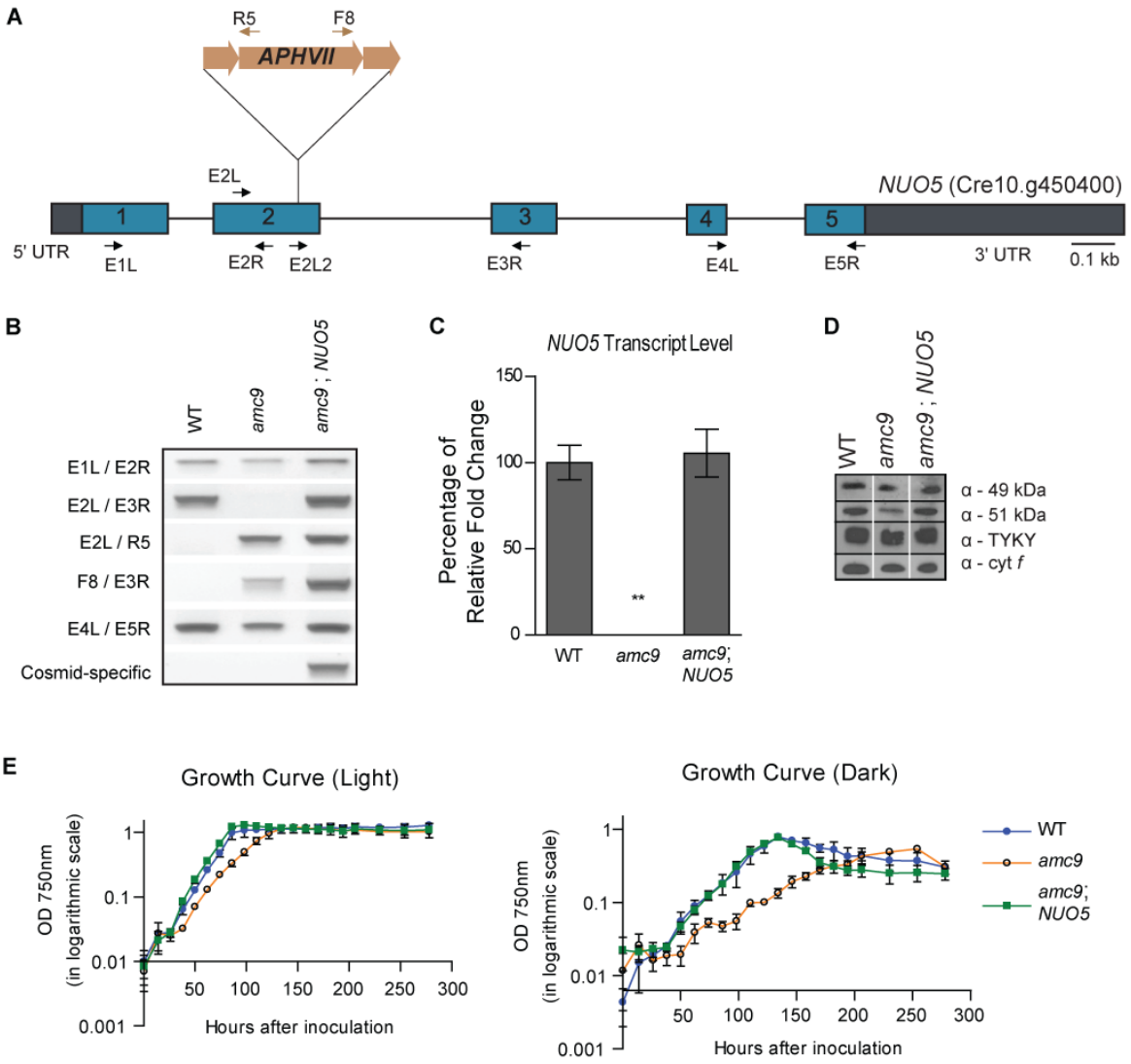

Supplemental Figure S4. The *NUO5* gene encoding the 24 kDa complex I subunit is disrupted in the *amc9* strain.

(A) A diagram of the *NUO5* gene with the approximate position of the insertional cassette in the *amc9* mutant is depicted here. The brown arrows indicate primers APH7R5 and APH7F8 that bind to the *APHVII* gene in the iHyg3 cassette. The black arrows represent *NUO5*-specific primers NUO5E1L, NUO5E2R, NUO5E2L, NUO5E2L2, NUO5E3R, NUO5E4L, and NUO5E5R (Table S1). (B) Diagnostic PCR of the *NUO5* gene in wild-type (WT, 4C$^-$), *amc9 (41D9)*, and one *amc9* strain transformed with a cosmid containing the *NUO5* gene [*amc9*; *NUO5*] is shown here. The positions of the primers used for diagnostic PCR of the *NUO5* gene are represented in (A). The location of the insertion was confirmed by amplification of the genomic region spanning the insertion site using primer pairs NUO5E2L / NUO5E3R.

A band of expected size (715 bp) was amplified in the wild-type and not in the *amc9* mutant. The insertion of the full-length iHyg3 cassette was confirmed by amplifying across the *NUO5/iHyg3* junctions in the *amc9* mutant. Primer pairs amplifying from the 5′-end (NUO5E2L / APH7-R5) and from the 3′-end (APH7-F8 / NUO5E3R) of the iHyg3 insertional cassette yielded products of expected size, 524 bp and 955 bp, respectively, in *amc9* but not in the wild-type. Diagnostic PCRs conducted upstream and downstream of the insertion site yielded amplicons of the expected size, indicating the absence of other major rearrangements in the *NUO5* gene of the *amc9* strain. Diagnostic PCR of the [*amc9; NUO5*] transformant revealed the presence of the wild-type *NUO5* gene, in addition to the endogenous disrupted *NUO5* gene. The primers (PH3 and 9A2 PH3, Table S1) were used for determining the presence of the cosmid (last row), harboring the wild-type *NUO5* gene. (C) Real-time quantitative PCR was used to assess the quantity of *NUO5* mRNA relative to the transcripts of three reference genes *TUA2, CBLP* and *UBI*. The average was obtained from three biological replicates, each including two technical replicates. The error bars represent standard deviation of the mean. The results are represented as percentage of fold change relative to WT (WT set to 100). Statistically significant difference with respect to the wild-type was determined by two-tailed unequal variances *t*-test. ** indicates $p < .01$. (D) SDS-PAGE immunoblotting was conducted on 10 µg of partially purified membranes using polyclonal antibodies to detect complex I soluble arm subunits: α- 49 kDa, α- 51 kDa, α- TYKY. α– cyt *f* was used to confirm equal loading. Vertical white lines indicate the assembly of different lanes from the same immunoblot. (E) The growth of WT ($4C^-$), *amc9* (41D9) and [*amc9*; *NUO5*] was recorded by measuring optical density at 750 nm, in the light (22 µmol m^{-2} s^{-1}) or in the dark, over a period of 10 days. The average of three biological replicates is reported here, with error bars indicating standard deviation of the mean.

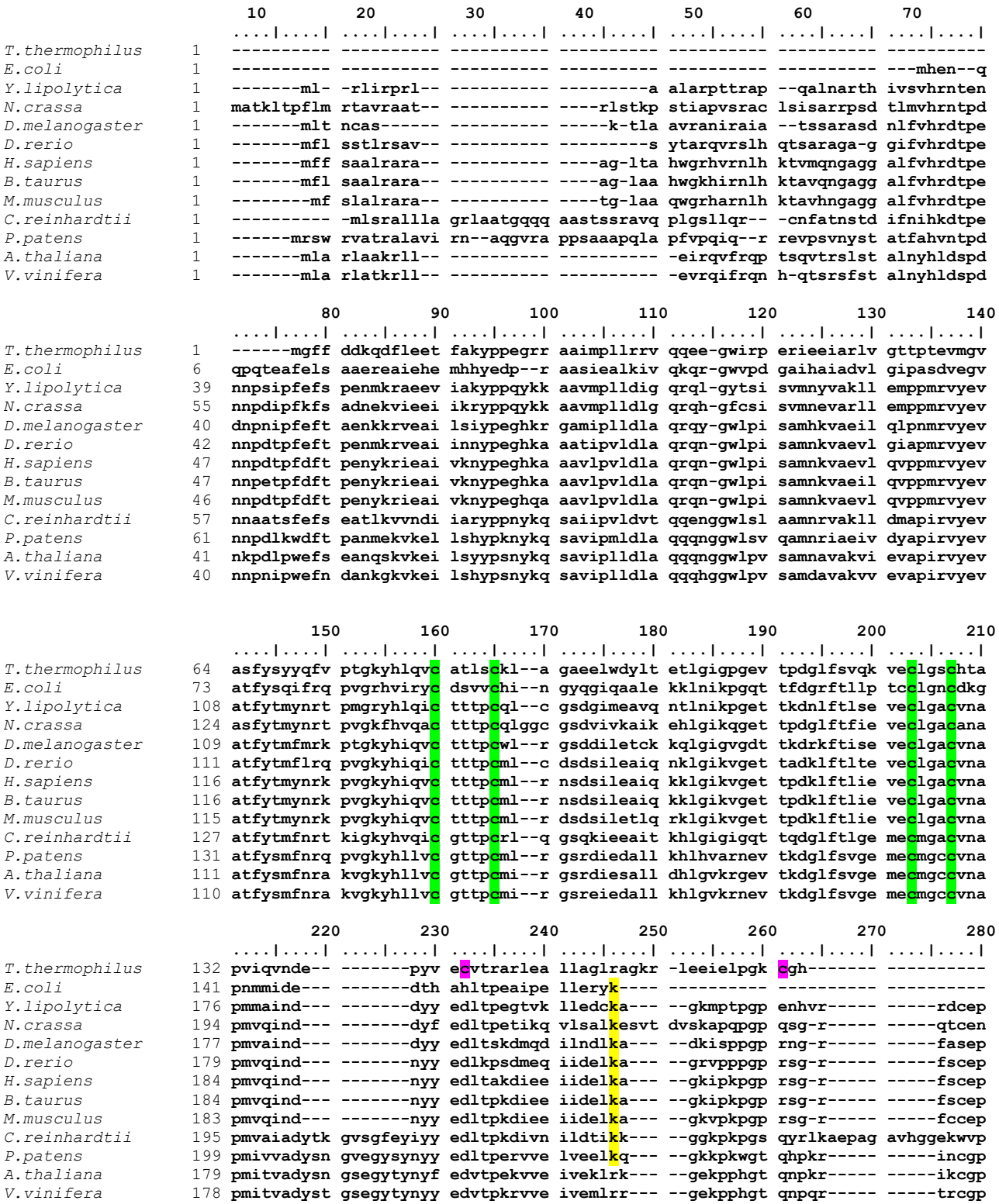
10 20 30 40 50 60 70
T.thermophilus 1 ---------- ---------- ---------- ---------- ---------- ---------- ----------
E.coli 1 ---------- ---------- ---------- ---------- ---------- ---------- ---mhen--q
Y.lipolytica 1 -------ml- -rlirprl-- ---------- ---------a alarpttrap --qalnarth ivsvhrnten
N.crassa 1 matkltpflm rtavraat-- ---------- ----rlstkp stiapvsrac lsisarrpsd tlmvhrntpd
D.melanogaster 1 -------mlt ncas------ ---------- -----k-tla avraniraia --tssarasd nlfvhrdtpe
D.rerio 1 -------mfl sstlrsav-- ---------- ---------s ytarqvrslh qtsaraga-g gifvhrdtpe
H.sapiens 1 -------mff saalrara-- ---------- ----ag-lta hwgrhvrnlh ktvmqngagg alfvhrdtpe
B.taurus 1 -------mfl saalrara-- ---------- ----ag-laa hwgkhirnlh ktavqngagg alfvhrdtpe
M.musculus 1 --------mf slalrara-- ---------- ----tg-laa qwgrharnlh ktavhngagg alfvhrdtpe
C.reinhardtii 1 ---------- -mlsrallla grlaatgqqq aastssravq plgsllqr-- -cnfatnstd ifnihkdtpe
P.patens 1 ------mrsw rvatralavi rn--aqgvra ppsaaapqla pfvpqiq--r revpsvnyst atfahvntpd
A.thaliana 1 -------mla rlaakrll-- ---------- ---------- -eirqvfrqp tsqvtrslst alnyhldspd
V.vinifera 1 -------mla rlatkrll-- ---------- ---------- -evrqifrqn h-qtsrsfst alnyhldspd
80 90 100 110 120 130 140
T.thermophilus 1 ------mgff ddkqdfleet fakyppegrr aaimpllrrv qqee-gwirp erieeiarlv gttptevmgv
E.coli 6 qpqteafels aaereaiehe mhhyedp--r aasiealkiv qkqr-gwvpd gaihaiadvl gipasdvegv
Y.lipolytica 39 nnpsipfefs penmkraeev iakyppqykk aavmplldig qrql-gytsi svmnyvakll emppmrvyev
N.crassa 55 nnpdipfkfs adnekvieei ikryppqykk aavmplldlg qrqh-gfcsi svmnevarll emppmrvyev
D.melanogaster 40 dnpnipfeft aenkkrveai lsiypeghkr gamiplldla qrqy-gwlpi samhkvaeil qlpnmrvyev
D.rerio 42 nnpdtpfeft penmkrveai innypeghka aatipvldla qrqn-gwlpi samnkvaevl giapmrvyev
H.sapiens 47 nnpdtpfdft penykrieai vknypeghka aavlpvldla qrqn-gwlpi samnkvaevl qvppmrvyev
B.taurus 47 nnpetpfdft penykrieai vknypeghka aavlpvldla qrqn-gwlpi samnkvaeil qvppmrvyev
M.musculus 46 nnpdtpfdft penykrieai vknypeghqa aavlpvldla qrqn-gwlpi samnkvaevl qvppmrvyev
C.reinhardtii 57 nnaatsfefs eatlkvvndi iaryppnykq saiipvldvt qqenggwlsl aamnrvakll dmapirvyev
P.patens 61 nnpdlkwdft panmekvkel lshypknykq savipmldla qqqnggwlsv qamnriaeiv dyapirvyev
A.thaliana 41 nkpdlpwefs eanqskvkei lsyypsnykq saviplldla qqqnggwlpv samnavakvi evapirvyev
V.vinifera 40 nnpnipwefn dankgkvkei lshypsnykq saviplldla qqqhggwlpv samdavakvv evapirvyev
150 160 170 180 190 200 210
T.thermophilus 64 asfysyyqfv ptgkyhlqvc atlsckl--a gaeelwdylt etlgigpgev tpdglfsvqk veclgschta
E.coli 73 atfysqifrq pvgrhviryc dsvvchi--n gyqgiqaale kklnikpgqt tfdgrftllp tcclgncdkg
Y.lipolytica 108 atfytmynrt pmgryhlqic tttpcql--c gsdgimeavq ntlnikpget tkdnlftlse veclgacvna
N.crassa 124 asfytmynrt pvgkfhvqac tttpcqlggc gsdvivkaik ehlgikqget tpdglftfie veclgacana
D.melanogaster 109 atfytmfmrk ptgkyhiqvc tttpcwl--r gsddiletck kqlgigvgdt tkdrkftise veclgacvna
D.rerio 111 atfytmflrq pvgkyhiqic tttpcml--c dsdsileaiq nklgikvget tadklftlte veclgacvna
H.sapiens 116 atfytmynrk pvgkyhiqvc tttpcml--r nsdsileaiq kklgikvget tpdklftlie veclgacvna
B.taurus 116 atfytmynrk pvgkyhiqvc tttpcml--r nsdsileaiq kklgikvget tpdklftlie veclgacvna
M.musculus 115 atfytmynrk pvgkyhiqvc tttpcml--r dsdsiletlq rklgikvget tpdklftlie veclgacvna
C.reinhardtii 127 atfytmfnrt kigkyhvqic gttpcrl--q gsqkieeait khlgigigqt tqdglftlge mecmgacvna
P.patens 131 atfysmfnrq pvgkyhllvc gttpcml--r gsrdiedall khlhvarnev tkdglfsvge mecmgccvna
A.thaliana 111 atfysmfnra kvgkyhllvc gttpcmi--r gsrdiesall dhlgvkrgev tkdglfsvge mecmgccvna
V.vinifera 110 atfysmfnra kvgkyhllvc gttpcmi--r gsreiedall khlgvkrnev tkdglfsvge mecmgccvna
220 230 240 250 260 270 280
T.thermophilus 132 pviqvnde-- -------pyv edvtrarlea llaglragkr -leeielpgk cgh------- ----------
E.coli 141 pnmmide--- -------dth ahltpeaipe lleryk---- ---------- ---------- ----------
Y.lipolytica 176 pmmaind--- -------dyy edltpegtvk lledcka--- --gkmptpgp enhvr----- -----rdcep
N.crassa 194 pmvqind--- -------dyf edltpetikq vlsalkesvt dvskapqpgp qsg-r----- -----qtcen
D.melanogaster 177 pmvaind--- -------dyy edltskdmqd ilndlka--- --dkisppgp rng-r----- -----fasep
D.rerio 179 pmvqind--- -------nyy edlkpsdmeq iidelka--- --grvpppgp rsg-r----- -----fscep
H.sapiens 184 pmvqind--- -------nyy edltakdiee iidelka--- --gkipkpgp rsg-r----- -----fscep
B.taurus 184 pmvqind--- -------nyy edltpkdiee iidelka--- --gkipkpgp rsg-r----- -----fscep
M.musculus 183 pmvqind--- -------nyy edltpkdiee iidelka--- --gkvpkpgp rsg-r----- -----fccep
C.reinhardtii 195 pmvaiadytk gvsgfeyiyy edltpkdivn ildtikk--- --ggkpkpgs qyrlkaepag avhggekwvp
P.patens 199 pmivvadysn gvegysynyy edltpervve lveelkq--- --gkkpkwgt qhpkr----- -----incgp
A.thaliana 179 pmitvadysn gsegytynyf edvtpekvve iveklrk--- --gekpphgt qnpkr----- -----ikcgp
V.vinifera 178 pmitvadyst gsegytynyy edvtpkrvve ivemlrr--- --gekpphgt qnpqr----- -----trcgp

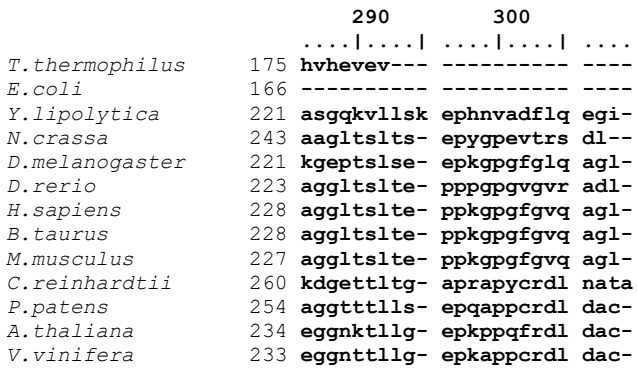

Supplemental Figure S5. Alignment of NUO5 / NDUFV2 / 24 kDa subunit orthologs.

NUO5 / NDUFV2 / 24 kDa subunit proteins were aligned using Clustal Omega (BLOSUM 62 scoring matrix) and Bioedit (Sievers *et al.*, 2011, Hall, 1999). The conserved cysteines that coordinate the 2Fe-2S (N1a) cluster in NUO5 are highlighted in green. In *E. coli*, the N1a cluster has a high midpoint redox potential implying a possible role in electron transfer through a flavosemiquinone intermediate (Verkhovskaya *et al.*, 2008). However, in mammalian complex I this cluster exhibits a low midpoint redox potential implying inability for electron relay and hence NDUFV2 is alternatively proposed to function in the structural stability of the enzyme (Birrell *et al.*, 2013, Verkhovskaya *et al.*, 2008). The two cysteines that provide increased stability by forming a disulfide in *T. thermophilus* ortholog are highlighted in magenta (Sazanov & Hinchliffe, 2006). The conserved lysine residue that is mutated to arginine in the Parkinson's disease patients (Nishioka *et al.*, 2010) is highlighted in yellow. NCBI accession numbers are as follows: *T. thermophilus* (AAA97942), *E. coli* (EDV69206), *Y. lipolytica* (XP_502254), *N. crassa* (XP_961535), *D. melanogaster* (NP_573228), *D. rerio* (NP_957041), *H. sapiens* (NP_066552), *B. taurus* (NP_776990), *M. musculus* (NP_082664), *C. reinhardtii* (XP_001698508), *P. patens* (XP_001759238), *A. thaliana* (NP_567244), *V. vinifera* (XP_002281655).

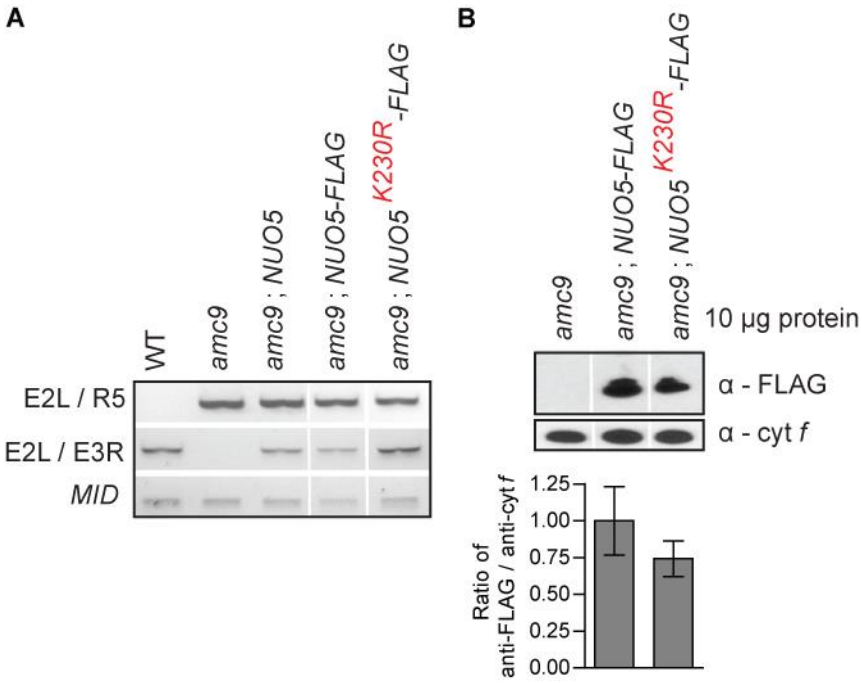

Supplemental Figure S6. The FLAG-tagged variants of NUO5 are expressed in the *amc9* mutant.

The *amc9* mutant was transformed with two constructs containing *NUO5* genomic DNA: i) wild-type *NUO5* sequence (*NUO5-FLAG*), or ii) mutant *NUO5* sequence encoding the K230R substitution (*NUO5*^{K230R}*-FLAG*). The wild-type (WT, 4C$^-$), *amc9* (*41D9*) mutant and [*amc9*; *NUO5*] strains were used as controls. White vertical thin lines indicate lanes that have been assembled together from the same gel. (A) Diagnostic PCR of the *NUO5* gene in the *amc9* transformants, at the site of insertion (NUO5 E2L / NUO5 E3R), resulted in amplification of wild-type sequence indicating the presence of transforming DNA. All transformants also contained the *amc9* insertional mutation (NUO5 E2L / APH7R5). The sequence and position of the primers is available in Table S1 and Figure S3. Amplification of the *MID* gene was used as control. (B) Immunoblotting was conducted on whole cell proteins separated by SDS-PAGE using monoclonal antibodies to detect FLAG tag (α- FLAG). Polyclonal antibody α– cyt *f* was used to test for equal loading. The proteins were quantified with ImageJ software from three independent biological replicates. No significant difference in NUO5-FLAG accumulation was observed for the wild-type NUO5-FLAG and the K230R NUO5-FLAG variant.

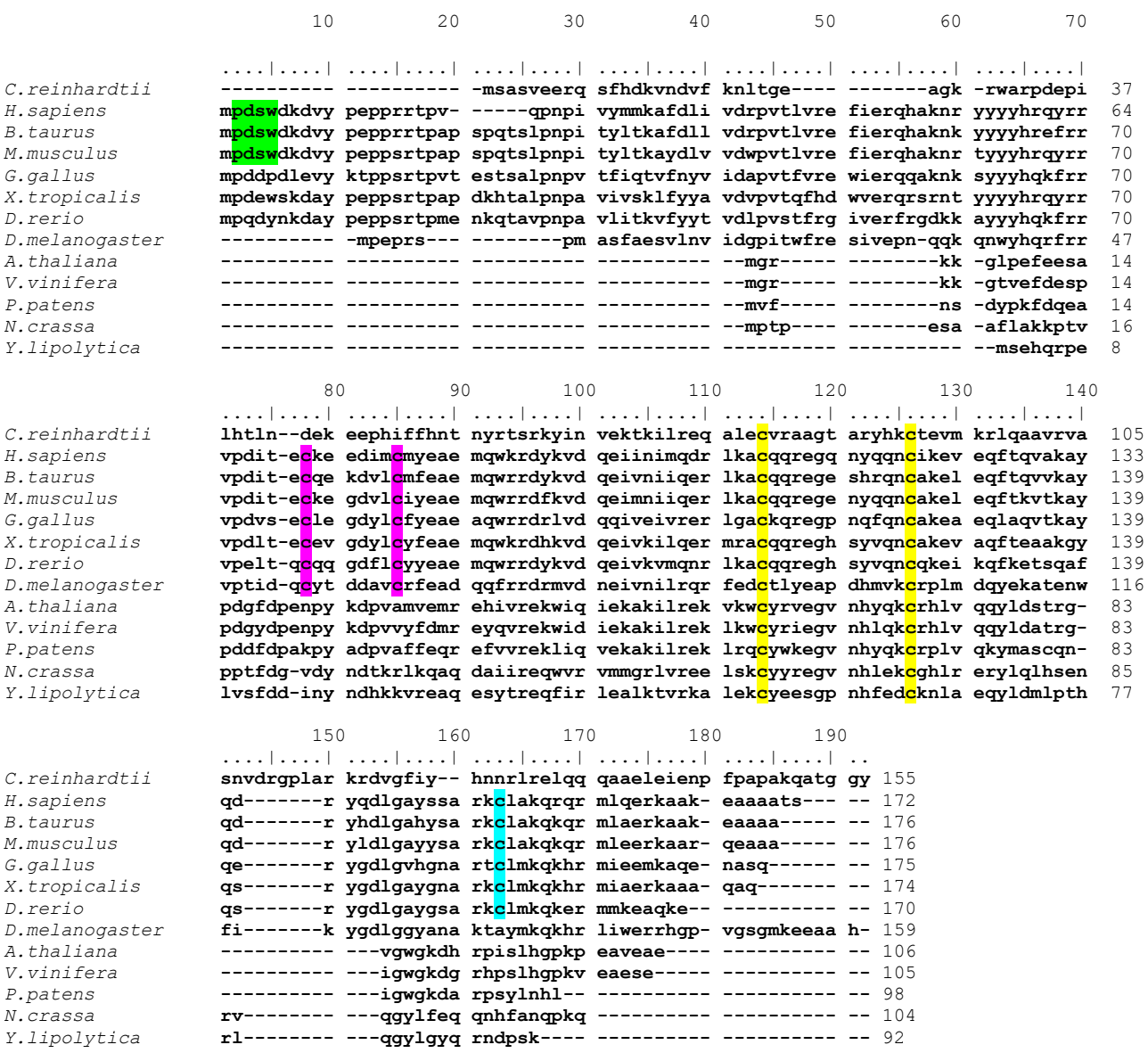

Supplemental Figure S7. Alignment of NUOB10 / NDUFB10 / PDSW subunits orthologs.

NUOB10 / NDUFB10 / PDSW subunit proteins were aligned using Clustal Omega (BLOSUM 62 scoring matrix) and Bioedit (Sievers *et al.*, 2011, Hall, 1999). The conserved PDSW sequence at the N-terminus is highlighted in green. The two cysteines of the C-$(X)_{11}$-C motif are highlighted in yellow, the C-$(X)_6$-C motif in pink and the fifth cysteine in the human ortholog is highlighted in blue. NCBI accession numbers are as follows: *D. melanogaster* (NP_651972), *G. gallus* (XP_414844), *H. sapiens* (O96000), *B. taurus* (Q02373), *M. musculus* (Q9DCS9), *X. tropicalis* (NP_001017250), *D. rerio* (Q6PC16), *C. reinhardtii* (XP_001694041), *P. patens* (XP_001770976), *A. thaliana* (NP_566608), *V. vinifera* (XP_002276810), *N. crassa* (CAA48768), *Y. lipolytica* (XP_002142991).

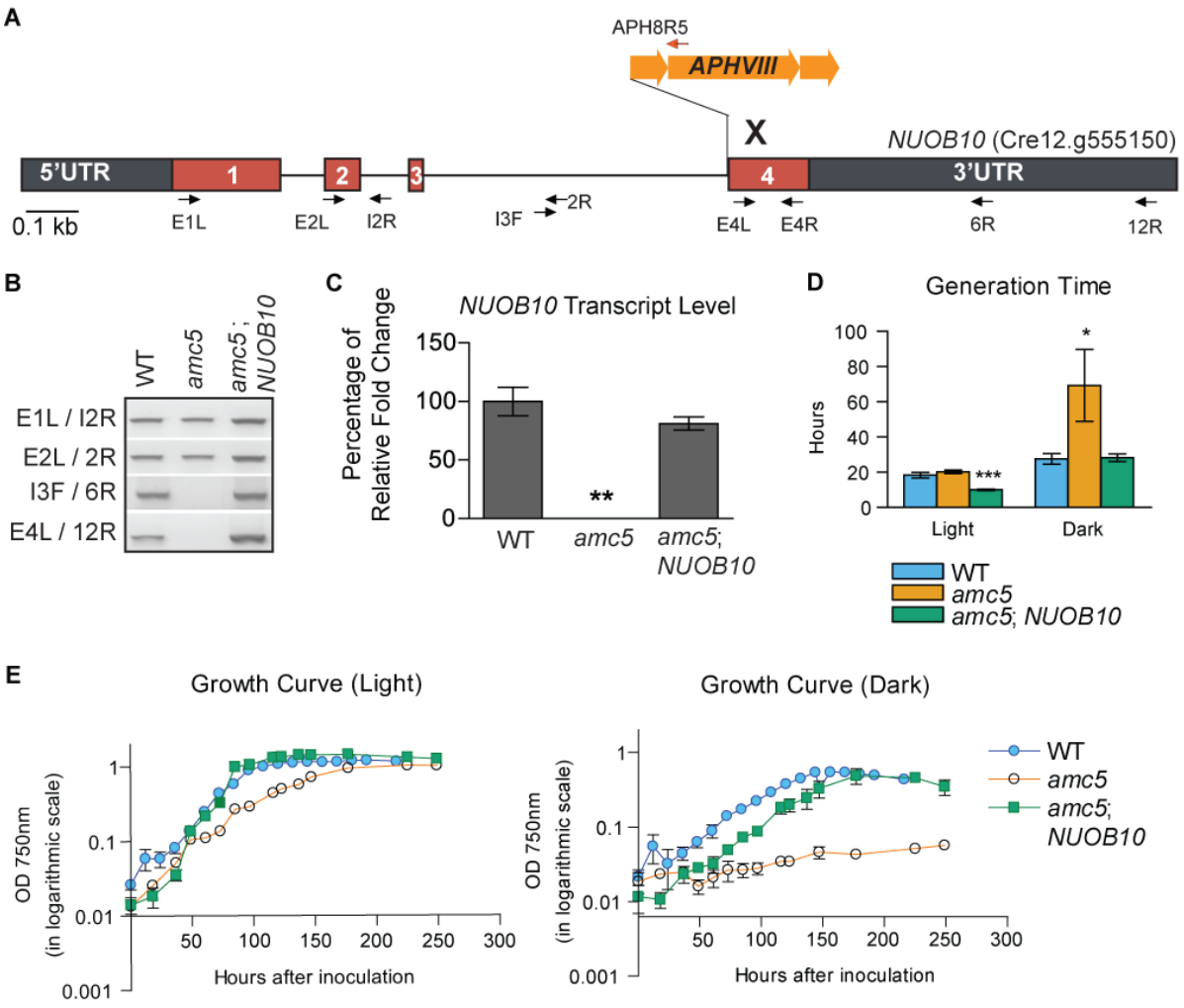

Supplemental Figure S8. The wild-type *NUOB10* gene restores heterotrophic growth to the *amc5* mutant.

(A) A diagram of the *NUOB10* gene with the position of the insertional cassette in the *amc5* mutant is depicted here. The gray and red rectangles represent UTRs and the coding sequence of *NUOB10*, respectively. The introns are denoted by thin black lines. The *X* mark indicates deletion of the *NUOB10* genomic region downstream of the insertion site. The black arrows indicate the primer binding sites for the *NUOB10*-specific primers and the orange primer is specific to the *APHVIII* insertional cassette conferring paromomycin resistance (iPm). (B) Diagnostic PCR of the *NUOB10* gene in the *amc5* strain reveals the presence of the molecular lesion as previously described in (Barbieri *et al.*, 2011). The [*amc5*; *NUOB10*] strain contains an intact copy of the *NUOB10* gene as expected. (C) Real - time RT-qPCR was used to assess the quantity of *NUOB10* mRNA relative to three reference genes *TUA2, CBLP* and *EIFA.*

The average was obtained from three biological replicates, each including two technical replicates. The error bars represent standard deviation of the mean. The results are represented as percentage of fold change relative to WT (WT set to 100). Statistical significance was determined with respect to wild-type by two-tailed unequal variance *t*-test. ** indicates *p*-value < .01. All primer sequences described in (A – C) are detailed in Supplementary Table S1. (D and E) The growth of the wild-type (WT, $3A^{+}$), *amc5* and [*amc5*; *NUOB10*] strains was recorded by measuring optical density at 750 nm, in the light or in the dark, over a period of 10 days. The average of three biological replicates is reported in (E), with error bars indicating standard deviation of the mean. The average generation time for each strain calculated from growth curves is depicted in (D). The error bars represent standard deviation of the mean. Statistical significance was determined by two-tailed equal variances *t*-test and * indicates *p*-value < .05, *** indicates *p*-value < .001.

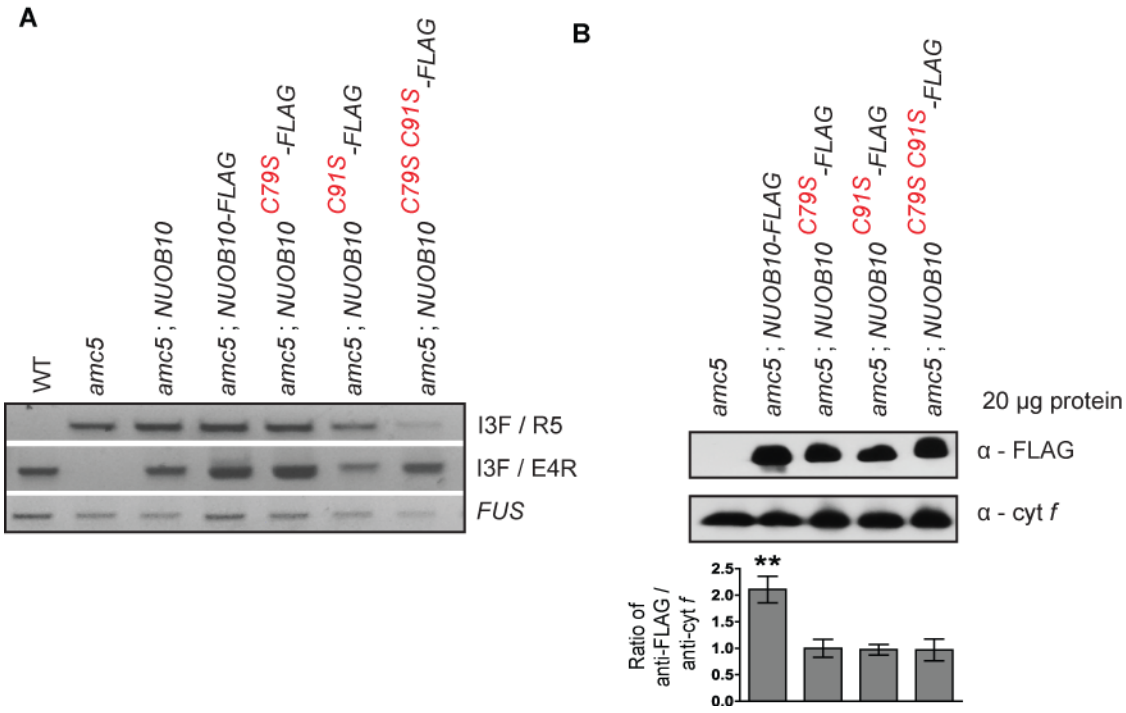

Supplemental Figure S9. The FLAG-tagged variants of NUOB10 are produced in the *amc5* mutant.

The *amc5* mutant was transformed with four constructs containing the *NUOB10* genomic DNA: i) wild-type *NUOB10* sequence (*NUOB10* or *NUOB10-FLAG*), and mutant *NUOB10* sequences encoding the variants with ii) the C79S substitution (*NUOB10*^{C79S}*-FLAG*), iii) the C91S substitution (*NUOB10*^{C91S}*-FLAG*), or iv) the C79S and C91S double substitutions (*NUOB10*^{C79SC91S}*-FLAG*). The wild-type (WT, 3A^{+}), *amc5* mutant and [*amc5*; *NUOB10*] strains were used as controls. (A) Diagnostic PCR of the *NUOB10* gene in the *amc5* transformants, at the site of insertion (NUOB10 I3F / NUOB10 E4R), shows amplification of wild-type sequence indicating the presence of transforming DNA. All transformants also contain the *amc5* insertional mutation (NUOB10 I3F/ APH8R5). The position of the primers is available in Figure S8A. Amplification of the *FUS* gene was used as control. (B) *(top):* SDS-PAGE immunoblotting was conducted on whole cell protein extract using monoclonal α- FLAG antibody to detect FLAG-tagged NUOB10. Polyclonal antibody to detect α– cyt *f* was used to test for equal loading. *(below):*The immunoblots were quantified by ImageJ software from three independent biological replicates (Schneider *et al.*, 2012). The transformant [*amc5*; *NUOB10-FLAG*] accumulates significantly more NUOB10-FLAG compared to other transformants with a $p < .01$ (calculated from three biological replicates using two-tailed unequal variances *t*-test).

Primer Name	Sequence (5' to 3')	Target
NUO5 E1L	AGCTAGCACCTCGTCTC	*NUO5*
NUO5 E2L	ACTACAAGCAGAGCGCCATC	
NUO5 E2R	GCTTAGCCACACGGTTC	
PmlI MKS /E2L2	CCGCACGAAAATTGGCAAGTACC	
NUO5 E3R	CATCTCGCCCAGTGTGAAC	
NUO5 E4L	CAACATCCTGGACACCATCAAG	
NUO5 E5R	GTTCAGGTCACGGCAGTAGG	
NUOB10 E1L	CGTCAAAGCTTCCACGATAAGG	*NUOB10*
NUOB10 E2L	CTGAGGGAGCAGGCTCTG	
NUOB10 I2R	CAGAGCCTGCTCCCTCAG	
PDSW-2R	TCATGCTTGCCCGAGAAG	
PDSW-9F	GTCATGAAGCGCCTGCAGG	
NUOB10 E4L	GGCTTCATCTACCACAACAACAG	
NUOB10 E4R	GAAAGGGTTCTCGATCTC	
NUOB10 I3F	CAGTTGGGGTGGGTCCTTC	
PDSW-6R	ATCGCACATGACGGCAG	
PDSW-12R	GAGGAGAGCAGTGGCATCGTG	
PH3	GGAGTCCCGGGATGGATTAAGG	9A2 Cosmid
9A2 PH3	GCCAGGCAACCGCGTCGAG	
APH7 F8	ACTGCTCGCCTTCACCTTC	iHyg3
APH7F	TCGATATCAAGCTTCTTTCTTGC	
APH7R	AAGCTTCCATGGGATGACG	
APH7 R3	AGAATTCCTGGTCGTTCCGCAG	
APH7 R4	TAGGAATCATCCGAATCAATACG	
APH7 R5	CGGTCGAGAAGTAACAGGG	
APH8R5	CACTCACAACCGGGATACC	iPm
AD1	NTCASTWTSGWGTT	Partially degenerate primer
CBLP-F	GCCACACCGAGTGGGTGTCGTGCG	*CBLP*
CBLP-R	CCTTGCCGCCCGAGGCGCACAGCG	
Tub-F	GTCCAAGCTGGGCTTCACCGTC	*TUA2*
Tub-R	GGCGGCAGATGTCGTAGATGGC	
Ubi lower	AGCGTCAGCGGCGGTTGCAGGTATCT	*UBI*
Ubi upper	GTACAGCGGCGGCTACAGGCAC	
EIF1A Fw	CATTGTGGAGCCGCCATTTC	*EIFA*
EIF1A Rev	GGCTGCTTGCATTTGCTTCC	

Supplemental Table S1: Sequence of primers used in this study. The sequence of primers used for TAIL-PCRs, diagnostic PCRs and RT-qPCRs are provided here. *NUO5, NUOB10, CBLP, TUA2, UBI, and EIF1A* are genes in the *Chlamydomonas* genome that correspond to the Phytozome v12 gene numbers

Cre10.g450400, *Cre12.g555150*, *Cre13.g599400* (also referred to as *Cre06.g278222)*, *Cre04.g216850*, *Cre03.g159200*, and *Cre02.g103550*, respectively.

Primer Name	Sequence (5' to 3')	Amplicon
pRS426-NUO5-F	GCGTATTTGACTAGTTCTAGAGCGGCCGCCACCGATTCACGCGTGTACTTG	A (1773 bp)
NUO5E2R	GCTTAGCCACACGGTTC	
NUO5E2L	ACTACAAGCAGAGCGCCATC	B (1532 bp)
NUO5-FLAG-R	GGCCGATTACTTGTCATCGTCGTCCTTATAGTCCGCGGTGGCGTTCAGGTC	
NUO5E2L	ACTACAAGCAGAGCGCCATC	C (1180 bp)
InfuK230R1	CTTGGGCTTGCCTCCCTTACGGATGGTGTCCAGGATGTTGACAATGTCCTTG	
InfuK230RF1	CAAGGACATTGTCAACATCCTGGACACCATCCGTAAGGGAGGCAAGCCCAAG	D (405 bp)
NUO5-FLAG-R	GGCCGATTACTTGTCATCGTCGTCCTTATAGTCCGCGGTGGCGTTCAGGTC	
NUO5-FLAG-F	GACTATAAGGACGACGATGACAAGTAATCGGCCGTGCTCGTG	E (677 bp)
NUO5-pRS426-R2	CAATTAACCCTCACTAAAGGGAACAAAAGCTGGTGATATGACCCAAGCTGCATATG	
pRS426-NUOB10-F	GCGTATTTGACTAGTTCTAGAGCGGCCGCCACCGCTTGCATCGTCCAGGGTAG	F (1734 bp)
C79SRev2	GCGCAGTGCCCGCAGCACGCACGCTCTCCAG	
pRS426-NUOB10-F	GCGTATTTGACTAGTTCTAGAGCGGCCGCCACCGCTTGCATCGTCCAGGGTAG	G (1767 bp)
C91SRev2	GTTGAGTTCCGCACCTCGGTGCTCTTGTGGTAC	
pRS426-NUOB10-F	GCGTATTTGACTAGTTCTAGAGCGGCCGCCACCGCTTGCATCGTCCAGGGTAG	H (1740 bp)
C79SC91SRev	GCTCTTGTGGTACCGCGCAGTGCCCGCAGCACGCACGCTCTCCAG	
pRS426-NUOB10-F	GCGTATTTGACTAGTTCTAGAGCGGCCGCCACCGCTTGCATCGTCCAGGGTAG	I (1780 bp)
NUOB10I2R	ATGTTGAGTTCCGCACCTC	
NUOB10E2L	CTGAGGGAGCAGGCTCTG	J (967 bp)
NUOB10-FLAG-R	CACGCTTTACTTGTCATCGTCGTCCTTATAGTCGTAGCCGCCAGTGGCCTG	
NUOB10-FLAG-F	GACTATAAGGACGACGATGACAAGTAAAGCGTGAGCGCAGCGTG	K (770 bp)
NUOB10-pRS426-R	CAATTAACCCTCACTAAAGGGAACAAAAGCTGGTACTGTAACGAGTACACAG	

C79S Fw NUOB10-FLAG-R	CTGGAGAGCGTGCGTGCTG CACGCTTTACTTGTCATCGTCGTCCTTATAGTCGTAGCCGCCAGTGGCCTG	L (946 bp)
C91S Fw NUOB10-FLAG-R	TACCACAAGTAGCACCGAGGTGCGGAAC CACGCTTTACTTGTCATCGTCGTCCTTATAGTCGTAGCCGCCAGTGGCCTG	M (908 bp)
C79SC91SFw NUOB10-FLAG-R	AGCGTGCGTGCTGCGGGCACTGCGCGGTACCACAAGAGCACCGAG CACGCTTTACTTGTCATCGTCGTCCTTATAGTCGTAGCCGCCAGTGGCCTG	N (946 bp)
APH7F-pRS426 APH7R-pRS426	TCGATAAGCTTGATATCGAATTCTCGATATCAAGCTTCTTTCTTG CCCTGGACGATGCAAGCGGTGGCGGCCGCTAAGCTTCCATGGGATGACG	iHyg3 (1796 bp)
APH8F2-pRS426 APH8R-pRS426	AAGTACACGCGTGAATCGGTGGCGGCCGCTCAGGCAGACGGGCAGGTG TCGATAAGCTTGATATCGAATTCCCTGGGTACCCGCTTCAAATAC	iPm (1902 bp)

Supplemental Table S2. Primers used for recombination-based cloning in yeast.

The sequence of primers used to amplify the overlapping DNA fragments by PCR is provided here. The nucleotide sequence encoding the FLAG-tag is in red. The site-directed mutations introduced into the primers are indicated with an underline. Each amplicon is given an alphabetical label for easy reference and its size is also provided in the last column.

The amplicons A to N were generated using *Chlamydomonas* genomic DNA (WT, 4C$^-$) as template. The iHyg3 and iPm amplicons were amplified using plasmids pHyg3 and pLS18 as templates, respectively (Berthold *et al.*, 2002, Depege *et al.*, 2003).

Clone Name	Fragments used for recombinant assembly
***In vivo* recombination in yeast**	
pRS426-ble-NUO5-WT-FLAG	pB-NA + A + B + E
pRS426-ble-NUO5-K230R-FLAG	pB-NA + A + C + D + E
pRS426-ble-NUOB10-WT-FLAG	pB-NA + I + J + K
pRS426-ble-NUOB10-C79S-FLAG	pB-NA + F + L + K
pRS426-ble-NUOB10-C91S-FLAG	pB-NA + G + M + K
pRS426-ble-NUOB10-C79SC91S-FLAG	pB-NA + H + N + K
In-Fusion HD cloning	
pRS426-iPm-NUO5-WT-FLAG	pRS426-ble-NUO5-WT-FLAG *Eco*RI, *Not*I (9 kb) + iPm
pRS426-iPm-NUO5-K230R-FLAG	pRS426-ble-NUO5-K230R-FLAG *Eco*RI, *Not*I (9 kb) + iPm
pRS426-iHyg3-NUOB10-WT-FLAG	pRS426-ble-NUOB10-WT-FLAG *Eco*RI, *Not*I (9 kb) + iHyg3
pRS426-iHyg3-NUOB10-C79S-FLAG	pRS426-ble-NUOB10-C79S-FLAG *Eco*RI, *Not*I (9 kb) + iHyg3
pRS426-iHyg3-NUOB10-C91S-FLAG	pRS426-ble-NUOB10-C91S-FLAG *Eco*RI, *Not*I (9 kb) + iHyg3
pRS426-iHyg3-NUOB10-C79SC91S-FLAG	pRS426-ble-NUOB10-C79SC91S-FLAG *Eco*RI, *Not*I (9 kb) + iHyg3

Supplemental Table S3. Method of plasmid construction.

The PCR fragments described in Table S2 carry overlapping segments that will enable recombinant cloning. The fragments used for generating each clone are detailed here. pB-NA refers to the vector pRS426-ble vector linearized (6864 bp) with *Not*I *and Ale*I restriction enzymes. The *NUO5* and *NUOB10* genes were cloned into the pRS426-ble vector by *in vivo* recombination in yeast. Subsequently, the *ble* selection marker was substituted by *in vitro* recombination using the In-Fusion HD enzyme.

Transformant name	**Recipient strain**	**Plasmid used for biolistic transformation**	**Selection marker**	**Selection medium**
amc9; *NUO5* [CC-5602]	*amc9 (41D9) strain* (*mt*$^-$; *nuo5::APHVII*; *arg7-8)* [CC-5601]	Cosmid 9A2 (contains wild-type *NUO5* gene, no tag)	*ARG7*	TAP
amc9; *NUO5-FLAG* [CC-5603]		pRS426-iPm-NUO5-WT-FLAG	*APHVIII*	TARG + Pm
amc9; *NUO5*^{K230R}*-FLAG* [CC-5604]		pRS426-iPm-NUO5-K230R-FLAG	*APHVIII*	TARG + Pm
amc5; *NUOB10* [CC-5592]	*amc5 (87D3)* strain (*mt*$^+$; *nuob10::APHVIII*; *arg7-8*) [CC-5591]	Cosmid 7D10 (contains wild-type NUOB10 gene, no tag)	*ARG7*	TAP
amc5; *NUOB10-FLAG* [CC-5593]		pRS426-iHyg3-NUOB10-WT-FLAG	*APHVII*	TARG + HyB
amc5; *NUOB10*^{C79S}*-FLAG* [CC-5594]		pRS426-iHyg3-NUOB10-C79S-FLAG	*APHVII*	TARG + HyB
amc5; *NUOB10*^{C91S}*-FLAG* [CC-5595]		pRS426-iHyg3-NUOB10-C91S-FLAG	*APHVII*	TARG + HyB
amc5; *NUOB10*$^{C79S\ C91S}$*-FLAG* [CC-5596]		pRS426-iHyg3-NUOB10-C79SC91S-FLAG	*APHVII*	TARG + HyB

Supplemental Table S4. Summary of biolistic transformation.

The *amc9* and *amc5* recipient strains were plated on the specified selective medium (column five) and bombarded with tungsten particles coated with the respective plasmids. Resulting transformants were screened by diagnostic PCR for the presence of the transgene and the

site-directed mutations were confirmed by sequencing. The transformant chosen for further analysis is indicated in column one. The recipient strain used for generating each transformant is provided in column two. The plasmids used to generate the transformants and the respective selection markers are detailed in columns three and four, respectively. The Chlamydomonas Resource Center reference numbers for the strains are provided in square brackets.

REFERENCES

Banroques, J., Delahodde, A., and Jacq, C. (1986) A mitochondrial RNA maturase gene transferred to the yeast nucleus can control mitochondrial mRNA splicing. *Cell* **46**: 837-844.

Barbieri, M.R., Larosa, V., Nouet, C., Subrahmanian, N., Remacle, C., and Hamel, P.P. (2011) A forward genetic screen identifies mutants deficient for mitochondrial complex I assembly in *Chlamydomonas reinhardtii*. *Genetics* **188**: 349-358.

Berthold, P., Schmitt, R., and Mages, W. (2002) An engineered *Streptomyces hygroscopicus aph 7*" gene mediates dominant resistance against hygromycin B in *Chlamydomonas reinhardtii*. *Protist* **153**: 401-412.

Birrell, J.A., Morina, K., Bridges, H.R., Friedrich, T., and Hirst, J. (2013) Investigating the function of [2Fe-2S] cluster N1a, the off-pathway cluster in complex I, by manipulating its reduction potential. *Biochem J* **456**: 139-146.

Chen, D.C., Yang, B.C., and Kuo, T.T. (1992) One-step transformation of yeast in stationary phase. *Curr Genet* **21**: 83-84.

de Montaigu, A., Sanz-Luque, E., Macias, M.I., Galvan, A., and Fernandez, E. (2011) Transcriptional regulation of CDP1 and CYG56 is required for proper NH4+ sensing in Chlamydomonas. *J Exp Bot* **62**: 1425-1437.

Depege, N., Bellafiore, S., and Rochaix, J.D. (2003) Role of chloroplast protein kinase Stt7 in LHCII phosphorylation and state transition in Chlamydomonas. *Science* **299**: 1572-1575.

Dreyfuss, B.W., Hamel, P.P., Nakamoto, S.S., and Merchant, S. (2003) Functional analysis of a divergent system II protein, Ccs1, involved in *c*-type cytochrome biogenesis. *J .Biol. Chem.* **278**: 2604-2613.

Hall, T.A. (1999) BioEdit: a user-friendly biological sequence alignment editor and analysis program for Windows 95/98/NT. *Nucleic Aciids Symposium Series* **41**: 95-98.

Harris, E.H., (1989) *The Chlamydomonas Sourcebook: A comprehensive guide to biology and laboratory use*. Academic Press, San Diego, CA.

Kropat, J., Hong-Hermesdorf, A., Casero, D., Ent, P., Castruita, M., Pellegrini, M., *et al.* (2011) A revised mineral nutrient supplement increases biomass and growth rate in Chlamydomonas reinhardtii. *Plant J* **66**: 770-780.

Livak, K.J., and Schmittgen, T.D. (2001) Analysis of relative gene expression data using real-time quantitative PCR and the 2(-Delta Delta C(T)) Method. *Methods* **25**: 402-408.

Newman, S.M., Boynton, J.E., Gillham, N.W., Randolph-Anderson, B.L., Johnson, A.M., and Harris, E.H. (1990) Transformation of chloroplast ribosomal RNA genes in Chlamydomonas: molecular and genetic characterization of integration events. *Genetics* **126**: 875-888.

Nishioka, K., Vilarino-Guell, C., Cobb, S.A., Kachergus, J.M., Ross, O.A., Hentati, E., *et al.* (2010) Genetic variation of the mitochondrial complex I subunit NDUFV2 and Parkinson's disease. *Parkinsonism Relat Disord* **16**: 686-687.

Noor-Mohammadi, S., Pourmir, A., and Johannes, T.W. (2014) Method for assembling and expressing multiple genes in the nucleus of microalgae. *Biotechnol Lett* **36**: 561-566.

Saint-Georges, Y., Bonnefoy, N., di Rago, J.P., Chiron, S., and Dujardin, G. (2002) A pathogenic cytochrome b mutation reveals new interactions between subunits of the mitochondrial bc1 complex. *J Biol Chem* **277**: 49397-49402.

Sambrook, J., Fritsch, E.F., and Maniatis, T., (1989) *Molecular Cloning A Laboratory Manual*. Cold Spring Harbor Laboratory Press, New York.

Sazanov, L.A., and Hinchliffe, P. (2006) Structure of the hydrophilic domain of respiratory complex I from *Thermus thermophilus*. *Science* **311**: 1430-1436.

Schneider, C.A., Rasband, W.S., and Eliceiri, K.W. (2012) NIH Image to ImageJ: 25 years of image analysis. *Nat Methods* **9**: 671-675.

Shimogawara, K., Fujiwara, S., Grossman, A., and Usuda, H. (1998) High-efficiency transformation of *Chlamydomonas reinhardtii* by electroporation. *Genetics* **148**: 1821-1828.

Sievers, F., Wilm, A., Dineen, D., Gibson, T.J., Karplus, K., Li, W., *et al.* (2011) Fast, scalable generation of high-quality protein multiple sequence alignments using Clustal Omega. *Mol Syst Biol* **7**: 539.

Verkhovskaya, M.L., Belevich, N., Euro, L., Wikstrom, M., and Verkhovsky, M.I. (2008) Real-time electron transfer in respiratory complex I. *Proc Natl Acad Sci U S A* **105**: 3763-3767.

Werner, R., and Mergenhagen, D. (1998) Mating Type Determination of *Chlamydomonas reinhardtii* by PCR. *Plant Mol. Biol. Rep,* **16**: 295-299.